The Journal of Immunology

Trypanosoma cruzi Infection Imparts a Regulatory Program in Dendritic Cells and T Cells via Galectin-1 –Dependent Mechanisms

Carolina V. Poncini, Juan M. Ilarregui, Estela I. Batalla, Steef Engels, Juan P. Cerliani, Marcela A. Cucher, Yvette van Kooyk, Stella M. González-Cappa and Gabriel A. Rabinovich

J Immunol published online 31 August 2015
http://www.jimmunol.org/content/early/2015/08/30/jimmunol.1403019

The Journal of Immunology is published twice each month by The American Association of Immunologists, Inc., 9650 Rockville Pike, Bethesda, MD 20814-3994.

Print ISSN: 0022-1767 Online ISSN: 1550-6606.

Published August 31, 2015, doi:10.4049/jimmunol.1403019

Trypanosoma cruzi Infection Imparts a Regulatory Program in Dendritic Cells and T Cells via Galectin-1–Dependent Mechanisms

Carolina V. Poncini,* Juan M. Ilarregui,[†,‡] Estela I. Batalla,* Steef Engels,[‡] Juan P. Cerliani,[†] Marcela A. Cucher,* Yvette van Kooyk,[‡] Stella M. González-Cappa,*[,1] and Gabriel A. Rabinovich[†,§,1]

Galectin-1 (Gal-1), an endogenous glycan-binding protein, is widely distributed at sites of inflammation and microbial invasion. Despite considerable progress regarding the immunoregulatory activity of this lectin, the role of endogenous Gal-1 during acute parasite infections is uncertain. In this study, we show that Gal-1 functions as a negative regulator to limit host-protective immunity following intradermal infection with *Trypanosoma cruzi*. Concomitant with the upregulation of immune inhibitory mediators, including IL-10, TGF-β1, IDO, and programmed death ligand 2, *T. cruzi* infection induced an early increase of Gal-1 expression in vivo. Compared to their wild-type (WT) counterpart, Gal-1–deficient (*Lgals1*$^{-/-}$) mice exhibited reduced mortality and lower parasite load in muscle tissue. Resistance of *Lgals1*$^{-/-}$ mice to *T. cruzi* infection was associated with a failure in the activation of Gal-1–driven tolerogenic circuits, otherwise orchestrated by WT dendritic cells, leading to secondary dysfunction in the induction of CD4$^+$CD25$^+$Foxp3$^+$ regulatory T cells. This effect was accompanied by an increased number of CD8$^+$ T cells and higher frequency of IFN-γ–producing CD4$^+$ T cells in muscle tissues and draining lymph nodes as well as reduced parasite burden in heart and hindlimb skeletal muscle. Moreover, dendritic cells lacking Gal-1 interrupted the Gal-1–mediated tolerogenic circuit and reinforced T cell–dependent anti-parasite immunity when adoptively transferred into WT mice. Thus, endogenous Gal-1 may influence *T. cruzi* infection by fueling tolerogenic circuits that hinder anti-parasite immunity. *The Journal of Immunology*, 2015, 195: 000–000.

Trypanosoma cruzi, the etiological agent of Chagas' disease, is a protozoan parasite that affects ∼10 million people in Latin America (1). *T. cruzi* infection is generally asymptomatic, but during chronicity one third of the patients develop dilated cardiomyopathy that could progress to heart failure due to the combined effects of parasite persistence, immune dysregulation, and microvascular damage (2). Despite several decades of research, the mechanisms underlying parasite-induced immunoregulation are only partially understood (3, 4). Studies using genetically deficient mice indicated that both CD4$^+$ and CD8$^+$ T cell populations are equally important for the control of parasitemia and host survival (5) and suggested the activation of immunoevasive programs that favor pathogen persistence and compromise the integrity of infected tissues (6–9). Both anti-inflammatory mediators, such as IL-10 and TGF-β, as well as immune inhibitory checkpoints, including programmed death ligand (PD-L)1 and PD-L2, play critical roles in dampening host immune responses during acute *T. cruzi* infection (9). Moreover, we and others have reported parasite-induced impairment of the Ag-presenting machinery and defects in effector T cell responses (10–12).

Despite their ability to orchestrate adaptive immune responses, dendritic cells (DCs) can also instruct the activation of tolerogenic circuits during infection, inflammation, and tissue injury (13–15). We recently demonstrated that *T. cruzi* trypomastigotes (Tp) may impart a tolerogenic program in bone marrow–derived DCs (BMDCs), which in response to the parasite, secrete high amounts of IL-10 and TGF-β1, synthesize low amounts of IL-12p70, and display lower T cell stimulatory capacity (16, 17).

Emerging evidence supports the critical role of glycan-binding proteins or lectins as host recognition molecules responsible for conveying pathogen-containing information into pro- or anti-inflammatory programs (18). Galectins, a family of β-galactoside–binding lectins, are highly conserved throughout animal evolution and play key roles in immune cell homeostasis. They are differentially expressed in peripheral tissues, sites of inflammation, and secondary lymphoid organs and modulate immune cell activation, differentiation, and survival (19). Galectin (Gal)-1, a prototype

*Instituto de Investigaciones en Microbiología y Parasitología Médicas, Facultad de Medicina, Universidad de Buenos Aires, Consejo Nacional de Investigaciones Científicas y Técnicas, C1121 Buenos Aires, Argentina; [†]Laboratorio de Inmunopatología, Instituto de Biología y Medicina Experimental, Consejo Nacional de Investigaciones Científicas y Técnicas, C1428 Buenos Aires, Argentina; [‡]Department of Molecular Cell Biology and Immunology, VU University Medical Center, 1081 HV Amsterdam, the Netherlands; and [§]Facultad de Ciencias Exactas y Naturales, Universidad de Buenos Aires, C1428 Buenos Aires, Argentina

[1]S.M.G.-C. and G.A.R. jointly supervised this study and should be considered as cosenior authors.

Received for publication December 2, 2014. Accepted for publication August 3, 2015.

This work was supported by grants from the Agencia Nacional de Promoción Científica y Tecnológica (Argentina), Consejo Nacional de Investigaciones Científicas y Técnicas (Argentina), Universidad de Buenos Aires (Argentina), Fundación Sales (Argentina), and Boehringer Ingelheim Fonds (Germany).

Address correspondence and reprint requests to Dr. Carolina V. Poncini, Instituto de Investigaciones en Microbiología y Parasitología Médicas, Facultad de Medicina, Universidad de Buenos Aires, Paraguay 2155, Piso 13, C1121 Buenos Aires, Argentina. E-mail address: cvponcini@gmail.com

The online version of this article contains supplemental material.

Abbreviations used in this article: BMDC, bone marrow–derived DC; DC, dendritic cell; dLN, draining lymph node; dpi, day postinfection; Gal, galectin; i.d.p., intradermoplantar; *Lgals1*$^{-/-}$, galectin-1–deficient; MHC II, MHC class II; PD-L, programmed death ligand; Tp, trypomastigote; Treg, T regulatory; WT, wild-type.

member of the galectin family, modulates a variety of immunological processes, including T cell viability (20), Th cell polarization (21), and host–pathogen interactions (22, 23), and blunts effector T cell responses in settings of autoimmunity, transplantation, and cancer (24). Particularly, Gal-1 activates a tolerogenic circuit in DCs mediated by IL-27 and IL-10 (25).

Galectins can also regulate microbial invasion by acting as pathogen recognition receptors, microbicidal agents, and modulators of innate and adaptive immunity (26, 27). For example, host cell–derived Gal-3 recognizes different pathogens such as *Leishmania major* and *Candida albicans* (28, 29), whereas Gal-4 and Gal-8 can bind and directly kill blood group Ag-positive bacteria (30). Interestingly, Gal-1 binds to Nipah virus envelope glycoproteins and confers protection by increasing antiviral immunity and inhibiting cell-to-cell fusion and viral fusion to endothelial cells (22, 31). Gal-1 also controls HIV replication (23) and Dengue virus infection (32). Furthermore, other studies suggested an important role for Gal-1 and Gal-3 in microbial adhesion and invasion to host cells and the extracellular matrix (33, 34). During *T. cruzi* infection, galectins display a wide expression pattern in a variety of infected cell types, including B cells, macrophages, and DCs (35–37). Notably, Gal-3 promotes binding of *T. cruzi* to coronary artery smooth muscle cells (33), and its expression is associated with myocarditis and fibrosis during chronic Chagas' disease (38). Moreover, a recent study demonstrated differential binding of human Gal-1, -3, -4, -7, and -8 to Tp and amastigotes compared with noninfective epimastigote forms present in the intestinal tract of the triatomine vector (39), reflecting changes in glycosylation during the metacyclogenesis and intracellular amastigote differentiation. Interestingly, whereas low concentrations of exogenously added Gal-1 promoted *T. cruzi* replication in vitro, high concentrations of this lectin inhibited its multiplication in infected macrophages (36). However, despite considerable progress, the pathophysiologic relevance of endogenous Gal-1 during the course of *T. cruzi* infection in vivo has not yet been explored.

In this study, we show that Gal-1 deficiency conferred resistance to acute *T. cruzi* infection in mice. Along with the upregulation of other immune inhibitory mediators, we found that Gal-1 expression was increased early after inoculation of *T. cruzi* parasites. Moreover, using the intradermoplantar (i.d.p.) route of infection, we found that *T. cruzi* triggered a tolerogenic circuit driven by Gal-1–expressing DCs, which blunted effector T cell responses and perpetuated parasite infection in host tissues. Thus, interruption of Gal-1–driven tolerogenic pathways during acute *T. cruzi* infection may promote parasite clearance and attenuate the severity of Chagas' disease.

Materials and Methods

Mice

Animal studies were approved by the local Institutional Animal Care Committee, School of Medicine, University of Buenos Aires. Male BALB/c, C3H/HeN, and CF1 mice were obtained from the animal facility of the Instituto de Investigaciones en Microbiología y Parasitología Médicas (School of Medicine, University of Buenos Aires). Male *Lgals1*$^{-/-}$ (C57BL/6 background) and C57BL/6 wild-type (WT) mice were housed and bred at the animal facilities of the School of Exact and Natural Sciences (University of Buenos Aires) until infection. Then, mice were housed at the animal facilities of the Instituto de Investigaciones en Microbiología y Parasitología Médicas according to respective institutional guidelines. For experiments performed at the Department of Molecular Cell Biology and Immunology (VU University Medical Center), mice were purchased from Charles River Laboratories. OT-II TCR transgenic (C57BL/6) mice were bred and housed at the VU University animal house under specific pathogen-free conditions. All experiments were performed according to institutional and national guidelines.

Parasites and infection

Infections were set up with a virulent *T. cruzi* strain (RA-Tc VI DTU) (12, 40, 41). The RA strain was used in all of the experiments. Tp were maintained by weekly i.p. inoculation of 3-wk-old male CF1 mice (1×10^5 parasites/mouse). For Tp purification, bloodstream forms were obtained from whole blood at the peak of parasitemia 7 d postinfection (dpi), thoroughly washed, and purified by density gradient centrifugation (Histopaque-1083, Sigma-Aldrich, St. Louis, MO) as previously reported (16). Labeling of Tp with CFSE was carried out using a 5 μM solution of CFDA-SE (Sigma-Aldrich) (16). Heat-killed parasites were prepared by incubation of purified parasites at 56˚C during 40 min. Tissue culture Tp were used for some experiments, including in vitro DC stimulation, cytokine detection, and mice infection, for confirmation purposes. Briefly, tissue culture Tp were maintained up to 2 mo in Vero cell line, cultured in RPMI 1640 medium with 5% heat-inactivated FCS, purified by centrifugation, and resuspended in PBS or medium depending on the assay. *T. cruzi* soluble Ags were obtained by mechanical lysis of cultured epimastigotes and used at 20 μg/ml. For the experimental infection, groups of 3–10 WT and *Lgals1*$^{-/-}$ mice (10–12 wk old) were infected by i.d.p. administration of 100 bloodstream Tp in the left hind footpad. Age-matched uninfected normal littermates injected with 20 μl vehicle (PBS–2% BSA) were used as control mice (noninfected). For i.p. inoculation, 100 bloodstream purified Tp were injected in 50 μl vehicle. Mortality was recorded daily and parasitemia was documented as previously described (42). Briefly, 10 μl fresh blood taken from mouse tail vein was incubated with 90 μl Tris-buffered 0.83% ammonium chloride (pH 7.2). Parasites were counted in a hemocytometer chamber and results were expressed as the number of Tp per milliliter of blood.

Reagents and recombinant Gal-1

LPS from *Escherichia coli* O26:B6 or 0111:B4 were from Sigma-Aldrich. Recombinant Gal-1 was obtained and purified as previously described (21). LPS was carefully removed by endotoxin-removing gel (Detoxi-Gel; Pierce) followed by analysis with a gel clot *Limulus* test (< 0.5 IU/mg; Associates of Cape Cod).

Cell purification and sample collection

For histological or immunological studies, animal samples were obtained from noninfected mice or after 9 or 16 dpi. After mechanical disaggregation in a 100-μm nylon cell strainer (BD Falcon), single-cell suspensions from spleens and/or lymph nodes were treated with ammonium potassium chloride phosphate buffer to lyse erythrocytes. When necessary, spleen mononuclear cells were purified by standard density gradient centrifugation on Histopaque-1083 (Sigma-Aldrich). T cells ($CD3^+$ or $CD4^+$) were purified from lymph nodes using anti-mouse biotin-conjugated CD4 or CD3 mAb (L3T4 and 145-2C11; BD Biosciences) and streptavidin-conjugated MicroBeads for magnetic positive selection (MiniMACS; Miltenyi Biotec). Naive OT-II $CD4^+$ T cells were purified from the spleen and lymph nodes using magnetic beads (Dynabead CD4 T cell negative isolation kit; Invitrogen) and CD62L MicroBeads (MiniMACS; Miltenyi Biotec). Splenic $CD11c^+$ DCs were purified from the mononuclear cell fraction using anti-mouse biotin-conjugated CD11c Ab (HL3; BD Biosciences) and streptavidin-conjugated MicroBeads for magnetic positive selection (Miltenyi Biotec). Purities were checked by flow cytometry and found to be ~97%. For isolation of skeletal or cardiac muscle infiltrates, single-cell suspensions were obtained after mechanical disaggregation of hearts or muscle tissue from the inoculated hind paw and followed by enzymatic digestion at 37˚C with hyaluronidase type IV-S (200 U/ml; Sigma-Aldrich) and collagenase type II (250 U/ml; Life Technologies/Invitrogen). Mononuclear cells were purified by density gradient centrifugation (Histopaque-1083; Sigma-Aldrich). Cell viability was assessed by trypan blue dye exclusion.

Generation of BMDCs

To obtain BMDCs, femurs and tibias from 8- to 12-wk-old mice were flushed and bone marrow cells were incubated for 7 d in IMDM complete medium supplemented with 10% (v/v) heat-inactivated FCS (Internegocios, Buenos Aires, Argentina), penicillin (100 U/ml) and streptomycin (100 mg/ml), and 2-ME (50 μM; referred as medium) with 20% conditioned medium from GM-CSF–producing J558 cells, as previously described (16). At day 7, cells were harvested by gentle pipetting, washed, plated (1×10^6 cells/ml) in 24-well plates (Nunc), and cultured in medium with or without LPS (5 μg/ml) in the presence or absence of live or heat-killed Tp (1:4 cell/parasite ratio) for 20 h. Control BMDCs were cultured with medium alone. In some experiments, BMDCs (1×10^6 cells/ml) were exposed to recombinant Gal-1 (10 μg/ml) in IMDM with 1 mM DTT and $CFSE^+$ Tp.

Allogeneic MLRs, OVA-specific proliferation assays, and T cell differentiation assays

For allogeneic MLRs, 1×10^5 $CD4^+$ or $CD3^+$ T cells purified from lymph nodes by positive selection (MiniMACS separation; Miltenyi Biotec) were cultured with 1×10^4 allogeneic WT or *Lgals1*$^{-/-}$-stimulated BMDCs in 96-well round-bottom plates (Orange Scientific). For blocking experiments, neutralizing Abs against IL-27p28 (AF1834; R&D Systems) or IL-10 (JES5-2A5; BD Biosciences) were added (10 μg/ml) at the beginning of cell culture. In secondary MLRs, naive $CD4^+$ T cells were primed in an MLR with LPS-stimulated BMDCs ($BMDCs_{LPS}$) or LPS-stimulated BMDCs exposed to Tp ($BMDCs_{Tp+LPS}$). After 5 d, primed T cells ($pCD4^+$) were purified by cell sorting ($CD3^+$) and added to a secondary MLR in the presence of control BMDCs plus naive $CD4^+$ T cells. For ex vivo alloresponse, $CD3^+$ T cells purified from lymph nodes of BALB/c mice and DCs isolated from spleens of noninfected or infected WT and *Lgals1*$^{-/-}$ mice were cultured for 96 h. In Ag-specific proliferation assays, OT-II $CD4^+$ T cells were cultured with syngeneic BMDCs prestimulated and pulsed with OVA for 18 h. To assess proliferation, experiments were performed in triplicate. Cultures were pulsed with 1 μCi [^{3}H]thymidine per well for the last 18 h and cells were harvested and counted using a Rack beta scintillation counter (Amersham Pharmacia Biotech). In some experiments, after 72 h of coculture, supernatants were collected and IL-10, IL-2, and IFN-γ were measured by ELISA as described above. For in vitro $CD4^+$ Th cell differentiation, C57BL/6 DCs (1×10^4) were cultured with LPS or with LPS in the presence of heat-killed Tp and 50 μg/ml OVA (Calbiochem) for 18 h in 96-well round-bottom plates (Orange Scientific). After washing, 5×10^5 purified naive $CD4^+$ T cells isolated from OT-II mice were added to each well. On day 2, recombinant mouse IL-2 (10 IU) was added. Cells were cultured for 6 d.

Flow cytometry and lectin-binding assay

Single-cell suspensions were incubated with fluorescence-labeled mAb for 30 min at 4°C. The following mAbs were used: isotype controls, allophycocyanin or PE–anti-CD11c (HL3, BD Biosciences or N418, Invitrogen) or FITC–anti-Gr-1 (RB6-8C5), allophycocyanin–anti-CD11b (M1/70), FITC–anti-CD4 (L3T4), allophycocyanin–anti-CD8 (Ly-2), PerCP–anti-CD3 (145-2C11) Abs (all from BD Biosciences) or PE-Cy5–anti-MHC class II (MHC II; M5/114.15.2) Abs from eBioscience or PE–anti-CD11c (N418), allophycocyanin–anti-CD11b (M1/70.15.11.5), PE-Vio770–anti-Ly6C (1G7.G10), PerCP–anti-CD8a (53-6.7), and PE–anti-Ki-67 (REA183) (all from Miltenyi Biotec). For intracellular staining, cells were treated with *T. cruzi* Ags as described above and brefeldin A (10 μg/ml; Sigma-Aldrich) for 5 h. After surface staining, cells were fixed and permeabilized with Cytofix/Cytoperm solution (BD Biosciences). The Abs used were isotype controls, PE–anti-IL-10 (JES5-16E3), PE–anti-IL-17A (TC11-18H10.1), and Alexa Fluor 647–anti-IFN-γ (XMG1.2) (all from BD Biosciences). For Foxp3 detection, cells were stained with anti-Foxp3 Ab (FJK-16s; eBioscience) or a T regulatory (Treg) cell detection kit (Miltenyi Biotec).

For lectin-binding assays, cells (5×10^5) were stained with FITC–Gal-1 (20 μg/ml) in the absence or presence of lactose (30 mM) or with biotinylated *Sambucus nigra* agglutinin (20 μg/ml; Vector Laboratories), peanut agglutinin (20 μg/ml; Sigma-Aldrich), or *Maackia amurensis* (MAL II, 10 μg/ml; Vector Laboratories) followed by PE-conjugated streptavidin (BD Biosciences) as described (20). Nonspecific binding was determined with PE-streptavidin alone. Cells were acquired on a FACSCalibur or a FACSAria flow cytometer (BD Biosciences) and analyzed using FlowJo 7.6 or WinMDI 2.9 software.

Cell death assays

Cell death was determined by staining with FITC-conjugated annexin V (BD Biosciences) and propidium iodide (Sigma-Aldrich) as described (20).

ELISA

Serum or cell supernatants were stored at −80°C until used according to the manufacturer's protocol. The IFN-γ ELISA set was from BD Biosciences. The IL-2, IL-10, IL-17, IL-27p28, and TNF ELISA kits were from R&D Systems.

Immunoblotting

Following overnight stimulation, cells were washed in PBS and treated with ice-cold lysis buffer (20 mM Tris-acetate [pH 7.0], 1 mM EGTA, 1% Triton X-100, 0.1 mM sodium fluoride, 5 μg/ml leupeptin, 1 mM sodium orthovanadate, 1 mM PMSF). Cell lysates were incubated on ice for 30 min, vortexed extensively, and centrifuged at 13,000 × *g* at 4°C for 10 min. The soluble fraction was removed and stored at −20°C until used. Samples were resuspended in Laemmli's buffer and boiled. Immunoblot analysis was performed as described (17). Equal amounts of protein (30 μg) were resolved by SDS-PAGE, blotted onto nitrocellulose membranes (GE Healthcare), and probed with anti–Gal-1 polyclonal Ab (3 μg/ml) generated as described (25) or anti–β-actin Ab (Abcam) followed by HRP-conjugated anti-rabbit or mouse IgG secondary Ab (Santa Cruz Biotechnology). Immunostaining was detected using ECL (GE Healthcare) according to the manufacturer's instructions. Band signal intensities were quantified by densitometry using Gel-Pro analyzer 4.0 software calculating arbitrary units relative to loading control.

Quantitative real-time RT-PCR

Total RNA from splenocyte single-cell suspensions was isolated using TRIzol reagent (Invitrogen Life Technologies) following the manufacturer's instructions. cDNA synthesis was performed with SuperScript III reverse transcriptase (Invitrogen Life Technologies). Quantitative real-time RT-PCR was performed using EvaGreen quantitative PCR mix plus (Solis BioDyne) or SYBR Green master mix (Applied Biosystems). Primers were: TGF-β1, 5′-GCTGAACCAAGGAGACGGAATA-3′ (forward) and 5′-GGGCTGATCCCGTTGATTT-3′ (reverse); IL-4, 5′-GAGCTCGTCTGTAGGGCTT-3′ (forward) and 5′-GACTCATTCATGGTGCAGC-3′ (reverse); Gal-1, 5′-TGAACCTGGGAAAAGACAGC-3′ (forward) and 5′-TCAGCCTGGTCAAAGGTGAT-3′ (reverse); Foxp3, 5′-TCCCACGCTCGGGTACAC-3′ (forward) and 5′-CCACTTGCAGACTCCATTTGC-3′ (reverse); GATA-3, 5′-ATGCCTGCGGACTCTAC-3′ (forward) and 5′-GGTGGTGGTGGTCTGAC-3′ (reverse); RORc, 5′-CTATCTGGGCAAGGCTACGGTT-3′ (forward) and 5′-CACAAAGCCAAACAATACGCG-3′ (reverse); T-bet, 5′-CAGGGAACCGCTTATATG-3′ (forward) and 5′-CTGGCTCTCCATCATTCA-3′ (reverse); PD-L2, 5′-TGCTCCTGCTGCCGATACT-3′ (forward) and 5′-GCCGACGTCTACGGTGTACA-3′ (reverse); IDO, 5′-GGGCTTCTTCCTCGTCTCTCTAT-3′ (forward) and 5′-CTTTCAGGTCTTGACGCTCTACTG-3′ (reverse). Samples were read using an ABI Prism 7500 sequencer detector (Applied Biosystems) and analyzed using the $2^{-\Delta\Delta CT}$ method. Results were normalized to GAPDH expression and expressed as mRNA arbitrary units or as fold change expression relative to control.

Histological analysis

On day 9 and 16 postinfection, hearts and skeletal muscle from the left hindlimb were fixed in 10% (v/v) formalin and embedded in paraffin. Noninfected animals were used as controls. Sections of 5 μm in thickness were stained with H&E. Quantification of the number of amastigote nests and the number of amastigotes per nest was estimated after the observation of at least 25 fields per preparation (set in triplicate with three to four preparations per mice) using a Nikon Eclipse E200 light microscope (×400–1000).

Confocal microscopy

Left popliteal lymph nodes (draining lymph nodes [dLNs]) were obtained from noninfected mice or after 2 d of mice infection. For immunostaining, lymph nodes were fixed with 4% paraformaldehyde and embedded in OCT. For confocal microscopy, Hoechst 33342 dye (Life Technologies) was used for nuclear staining together with the following primary Abs: rabbit anti–Gal-1 IgG (25), rat anti–CD4-FITC (553047; BD Pharmingen), rat anti-CD8 (ab22378; Abcam), rat anti–CD11c-FITC (117306; BioLegend), mouse anti–α-SMA (1A4; Dako). Secondary Abs used were anti-rat IgG–Alexa Fluor 488 (Vector Laboratories; 1:500), anti-rabbit IgG–Alexa Fluor 555 (Cell Signaling Technology; 1:1000) and anti-mouse IgG–Alexa Fluor 488 (Cell Signaling Technology; 1:1000).

Adoptive transfer assays

After enzymatic treatment of spleens with collagenase D and DNase I (1 mg/ml and 20 μg/ml, respectively; Sigma-Aldrich) and preparation of single-cell suspensions, splenic DCs from early infected (7 dpi) WT or *Lgals1*$^{-/-}$ mice were sorted and transferred i.p. into WT animals (1×10^6 cells/mouse). Although parasites were not detected in donor DCs, we inoculated 100 RA-Tp immediately after i.p. DC injection to synchronize adoptive transfer and parasite inoculation. Parasitemia was evaluated every 3–5 d and mortality was recorded daily. Immunological responses were evaluated at 14 dpi.

Statistical analysis

Two groups were compared with an unpaired Student *t* test. For multiple comparisons, one-way ANOVA and a Tukey post hoc test or two-way ANOVA and Bonferroni post hoc correction were performed to analyze

statistical significance. Survival was analyzed by Kaplan–Meier. Analyses were carried out using GraphPad Prism 4 software for Windows. A p value <0.05 was considered significant.

Results

Mice lacking Gal-1 show enhanced resistance to acute T. cruzi *infection and display low parasite burden in muscle tissue*

We first assessed whether Gal-1 deficiency influences the control of parasite burden and mice susceptibility to *T. cruzi* infection. For this purpose, Gal-1–deficient (*Lgals1*$^{-/-}$) and WT mice were infected via i.d.p. route with *T. cruzi* Tp (RA strain). Whereas no differences were observed in blood parasitemia between Gal-1–deficient and WT mice until day 20 postinfection (Fig. 1A), *Lgals1*$^{-/-}$ animals survived longer and 20% reached the chronic stage of infection (Fig. 1B). Of note, these animals successfully controlled parasite load, and even after 50 dpi they still displayed low parasite counts using ultrasensitive methods (microhematocrit) (data not shown). As susceptibility to *T. cruzi* could be the result of an imbalance between inflammation, uncontrolled parasite multiplication, and tissue damage (8), we assessed these

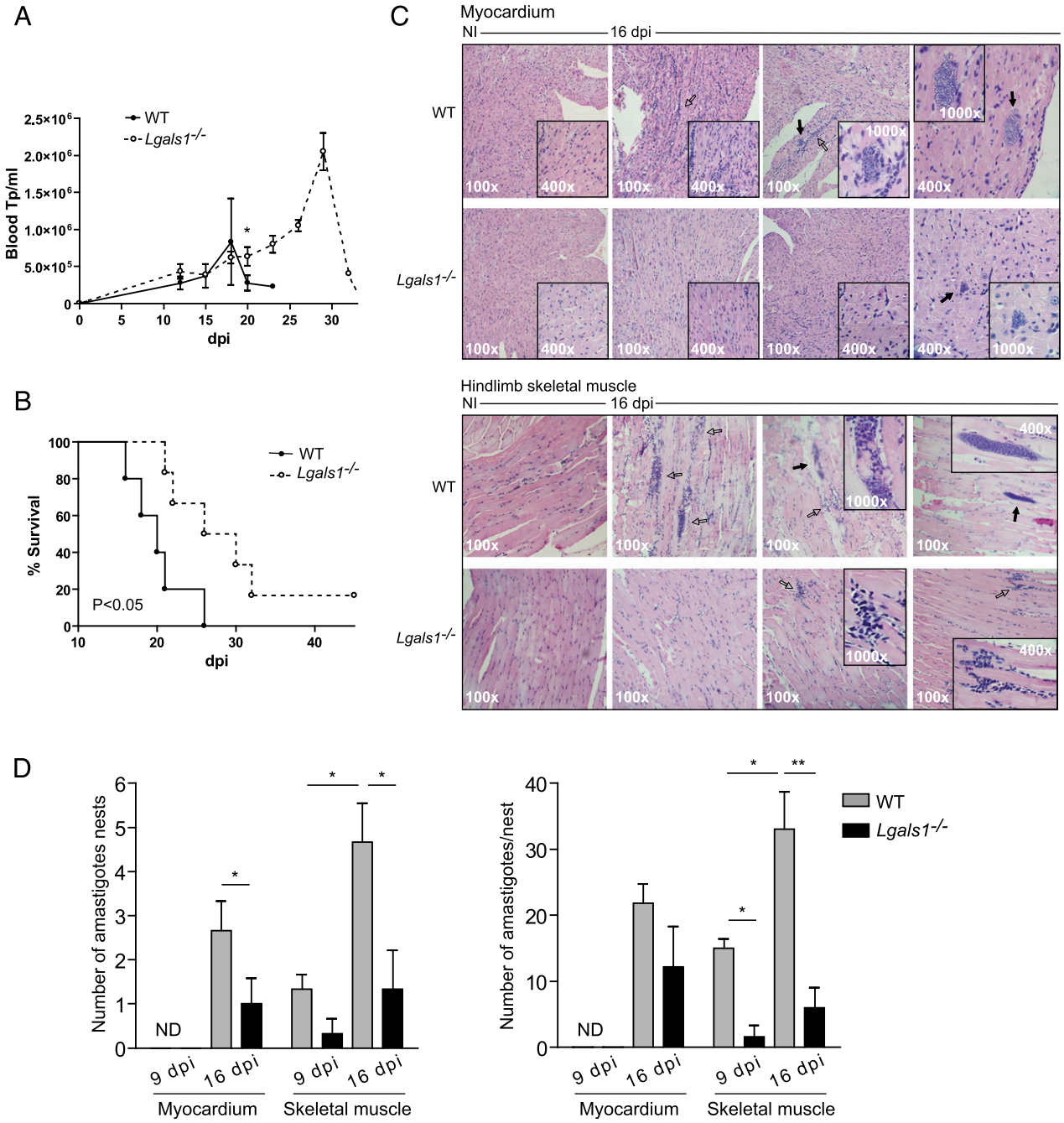

FIGURE 1. Gal-1 deficiency confers resistance to *T. cruzi* infection. (**A** and **B**) *Lgals1*$^{-/-}$ (○) and WT mice (●) were infected in the left hind footpad via i.d.p. route with 100 RA blood-Tp. Peripheral blood parasitemia (A) and survival curves (B) were analyzed during acute infection. A representative experiment of four performed with 5–10 mice per group is shown. Parasitemia is expressed as mean ± SEM. *$p < 0.05$, unpaired Student t test and Kaplan–Meier. (**C**) H&E staining of cardiac and hindlimb skeletal muscle from noninfected (NI) or infected (16 dpi) mice. Closed arrows show amastigotes nests; open arrows indicate mononuclear cell infiltrates. (**D**) Quantification of the number of amastigotes nests (*left panel*) and the average number of amastigotes per nest (*right panel*). At least 25 fields per section were analyzed (three to four sections or slices per mouse). Results are expressed as mean ± SEM from two experiments performed with three mice per group. *$p < 0.05$, **$p < 0.01$, two-way ANOVA and Bonferroni posttest. ND, nondetectable.

parameters in *Lgals1*$^{-/-}$ and WT mice. Histopathologic analysis revealed higher parasite load, measured as number of amastigotes nests and amastigotes per nest, in myocardium and hindlimb skeletal muscle from WT compared with *Lgals1*$^{-/-}$-infected mice (Fig. 1C, 1D). These data suggest that Gal-1 controls susceptibility to *T. cruzi* infection in vivo.

Endogenous Gal-1 is upregulated during T. cruzi *infection and modulates cytokine production*

In previous studies, we found that Gal-1 expression was greater during the peak and resolution of autoimmune inflammatory responses (25). In this study, we found that Gal-1 mRNA and Gal-1 protein were upregulated in the spleen of infected mice at days 9 and 16 postinfection compared with noninfected mice (Fig. 2A, 2B). This effect was accompanied by augmented expression of TGF-β1 and IL-4 mRNA at 9 dpi (Fig. 2C).

To understand the function of endogenous Gal-1 during *T. cruzi* infection, we then examined cytokine production in sera and splenocyte culture supernatants from *Lgals1*$^{-/-}$ versus WT mice. Parasite infection resulted in increased amounts of IFN-γ and IL-10 in samples from both WT and *Lgals1*$^{-/-}$ mice (Fig. 2D). However, whereas *Lgals1*$^{-/-}$ mice showed more IFN-γ in serum at 9 dpi, WT mice exhibited augmented IL-10 production in both culture supernatants and serum at 9 and 16 dpi, respectively (Fig. 2D). Additionally, we found no significant production of IL-17A during infection and no difference in the amounts of TNF between WT and *Lgals1*$^{-/-}$ mice (data not shown).

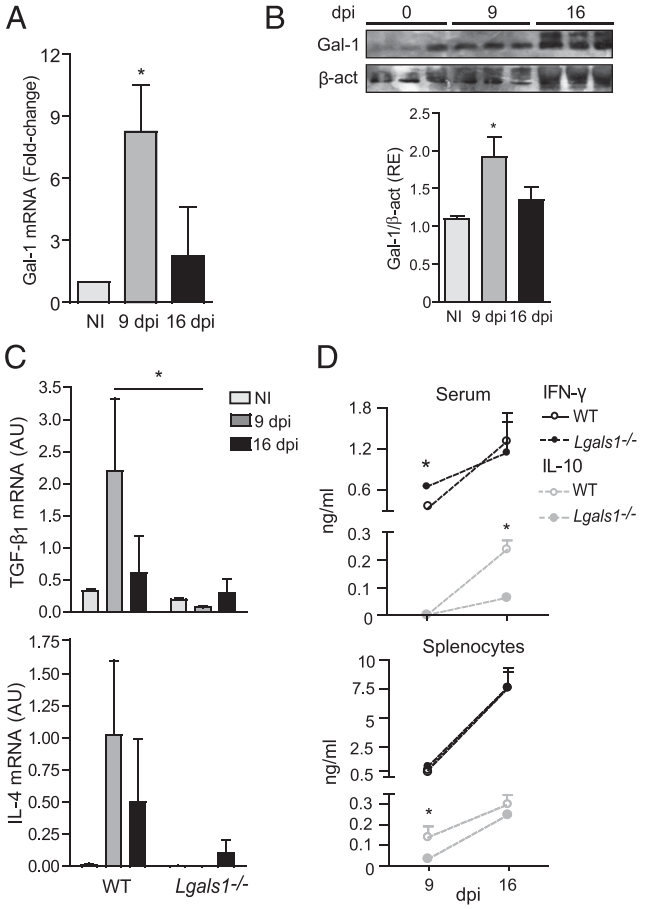

FIGURE 2. Endogenous Gal-1 is upregulated during *T. cruzi* infection and modulates cytokine production. *Lgals1*$^{-/-}$ and WT mice were infected via the i.d.p. route as described in Fig. 1. Relative Gal-1 mRNA (**A**) and protein (**B**) expression in splenocytes at days 0, 9, or 16 postinfection by quantitative real-time RT-PCR and immunoblot analysis, respectively. *$p < 0.05$, one-way ANOVA and Tukey posttest. (**C**) Total RNA was obtained from splenocytes and TGF-β1 (*upper panel*) and IL-4 (*lower panel*) mRNAs were measured by quantitative real-time RT-PCR. Results are presented relative to GAPDH mRNA and expressed as mean ± SEM (n = 5/condition, three independent experiments). *$p < 0.05$, two-way ANOVA and Bonferroni posttest. (**D**) IFN-γ and IL-10 were measured in serum (*upper panel*) and in splenocyte culture supernatants (*lower panel*) at 9 or 16 dpi by ELISA. Data are representative of five independent experiments with three replicates per group. *$p < 0.05$, WT versus *Lgals1*$^{-/-}$ (unpaired Student t test).

Endogenous Gal-1 controls T cell responses during T. cruzi *infection*

Because Gal-1 selectively regulates the viability of Th1 and Th17 cells through glycosylation-dependent mechanisms (20) and parasite infection results in spleen enlargement as a consequence of augmented lymphocyte polyclonal responses (9), we investigated the impact of Gal-1 deletion in shaping the T cell compartment during *T. cruzi* infection. We found enhanced cellularity in the spleen of *Lgals1*$^{-/-}$ mice compared with their WT counterpart at 9 dpi as evidenced by the increased number of viable cells (Fig. 3A) and larger spleen size (Fig. 3B). Notably, the lower cell count in spleens of infected WT mice correlated with increased annexin V (Fig. 3C) and propidium iodide (data not shown) staining of splenocytes. In this regard, WT but not *Lgals1*$^{-/-}$ mice experienced a decline in CD4$^+$ T cells counts in the spleen in response to infection (Fig. 3D). Interestingly, contraction of the CD4$^+$ T cell compartment was accompanied by enhanced Foxp3 and GATA-3 mRNA expression in infected WT mice (Fig. 3E). However, we found no significant changes in the expression of the transcription factors RORc and T-bet, associated with Th17 and Th1 subsets, respectively, at 9 or 16 dpi (Fig. 3E), suggesting a selective role of Gal-1 in the control of effector and Treg cell responses during *T. cruzi* infection. Of note, when we compared the repertoire of glycan structures (glycophenotype) present on the surface of noninfected versus infected WT and *Lgals1*$^{-/-}$ splenocytes, we only found a significant increase in the binding of biotinylated peanut agglutinin, a plant lectin that recognizes asialo core 1 *O*-glycans, in splenic CD4$^+$ T cells from infected *Lgals1*$^{-/-}$ mice (Supplemental Fig. 1), probably reflecting an increase in their activation status (20).

Because Gal-1 also influences the differentiation, expansion, and functional properties of Treg cells (21, 43, 44), we also analyzed the CD4$^+$Foxp3$^+$ T cell compartment in the spleens of noninfected and infected mice. In the absence of infection, WT mice displayed a discrete but slightly larger population of CD4$^+$Foxp3$^+$ T cells as compared with *Lgals1*$^{-/-}$ mice (Fig. 3F). Interestingly, *T. cruzi* infection considerably enhanced the frequency of CD4$^+$Foxp3$^+$ T cells in WT, but not in *Lgals1*$^{-/-}$, animals (Fig. 3F), suggesting that endogenous Gal-1 may favor Treg cell differentiation or may promote their recruitment to the spleen during parasite infection.

The augmented frequency of CD4$^+$Foxp3$^+$ Treg cells in the spleen of WT-infected mice was accompanied by increased parasite load in hindlimb skeletal muscle and heart (Fig. 1C, 1D). Although we found no significant differences in the frequency of CD8$^+$ T cells in spleens from WT and *Lgals1*$^{-/-}$ mice, the latter displayed a higher number of these cells in muscle infiltrates at day 16 postinfection (Fig. 4A). Cellular infiltrates in hindlimb skeletal muscle and heart from infected animals were found to be enriched with mononuclear cells (Fig. 4A), and only a third part of the total number of cells recovered from WT mice could be obtained from *Lgals1*$^{-/-}$ animals (data not shown), demonstrating that lower parasite load was accompanied by diminished number of infiltrating cells. Interestingly, cellular infiltrates in *Lgals1*$^{-/-}$ mice exhibited a higher number of IFN-γ–producing CD4$^+$ T cells

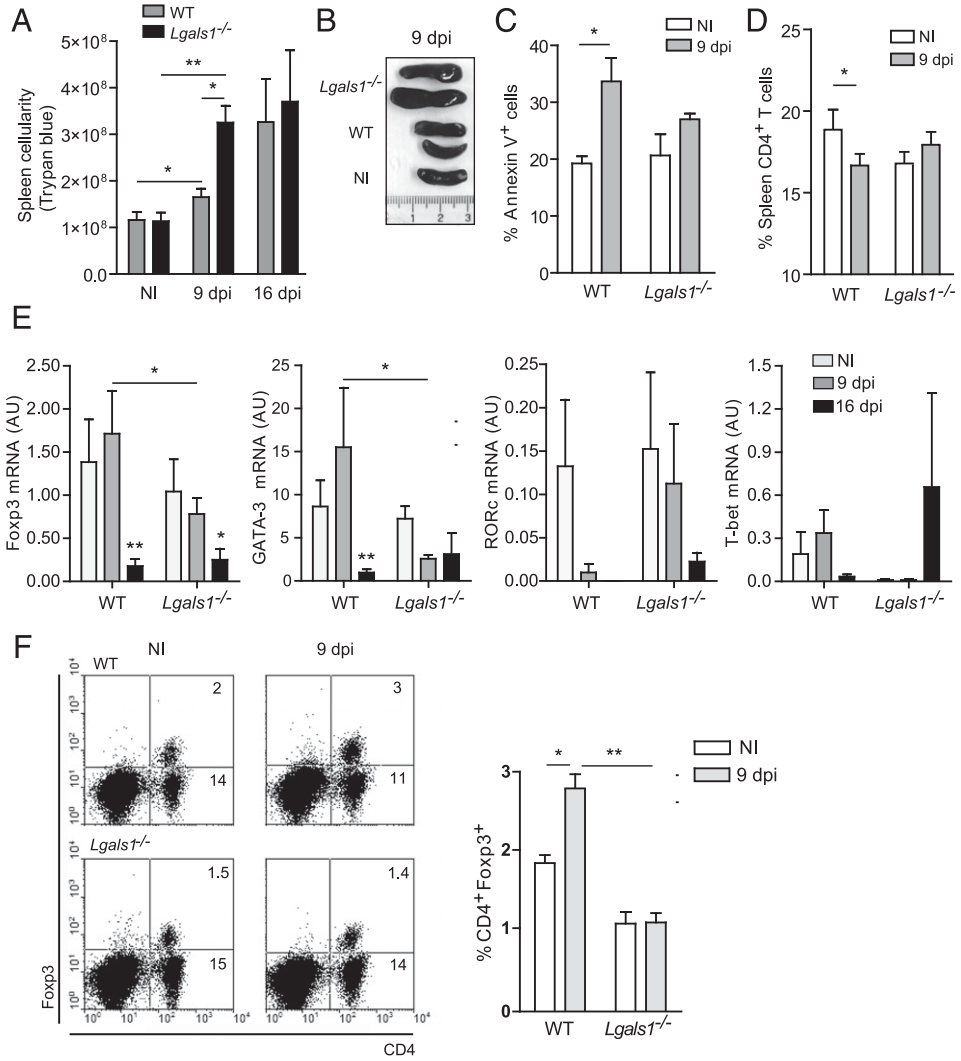

FIGURE 3. Gal-1 deficiency reshapes spleen cellularity and frequency of $CD4^+Foxp3^+$ T cells in *T. cruzi*–infected mice. (**A**–**F**) Splenocytes were obtained from noninfected (NI) or infected animals at days 9 or 16 after Tp inoculation. (A) Total splenocyte number and viability in WT and *Lgals1*$^{-/-}$ mice were determined by trypan blue dye exclusion. (B) Dissected spleens from WT and *Lgals1*$^{-/-}$ mice obtained at 9 dpi. Annexin V staining (C) and frequency of splenic $CD4^+$ T cells (D) were determined by flow cytometry. Propidium iodide staining revealed a similar tendency (data not shown). Results are expressed as mean ± SEM of seven independent experiments. *$p < 0.05$, **$p < 0.01$, unpaired Student *t* test and ANOVA for multiple comparisons. (E) Total RNA was obtained from WT and *Lgals1*$^{-/-}$ splenocytes and analyzed for Foxp3, GATA-3, RORc, and T-bet mRNA by quantitative real-time RT-PCR (n = 5/group, three independent experiments). Statistical analysis was performed using two-way ANOVA followed by a Bonferroni posttest. *$p < 0.05$, **$p < 0.01$, NI versus infected or WT versus *Lgals1*$^{-/-}$. (F) Frequency of $CD4^+Foxp3^+$ T cells at 9 dpi analyzed by flow cytometry. One representative set of dot plots (*left panels*) and the summary data of three independent experiments (mean ± SEM; *right panel*) are shown. *$p < 0.05$, **$p < 0.01$, NI versus infected or WT versus *Lgals1*$^{-/-}$ (two-way ANOVA and Bonferroni posttest).

when stimulated with *T. cruzi* Ags in vitro (Fig. 4B). Additionally, at 16 dpi popliteal lymph nodes from *Lgals1*$^{-/-}$-infected mice showed an increased frequency of $CD4^+$ T cells (Fig. 4C) along with a considerable decline in the percentage of $CD4^+CD25^+$ $Foxp3^+$ Treg cells (Fig. 4D) and enhanced T cell proliferation as determined by Ki-67 staining (Fig. 4E). These results suggest that Gal-1 may favor *T. cruzi* persistence in infected hosts by limiting Th1 responses and enhancing Treg cell function.

T. cruzi-*stimulated BMDCs favor the in vitro differentiation of a population of CD4*$^+$*Foxp3*$^+$ *Treg cells with enhanced suppressive potential*

Previous studies demonstrated that Gal-1 triggers an immunoregulatory circuit mediated by IL-27–producing DCs and IL-10–secreting $CD4^+$ T cells, which blunt Th1 and Th17 responses and promote the resolution of autoimmune inflammation (25). Interestingly, a number of tolerogenic stimuli, including vasoactive intestinal peptide, vitamin D_3, and IL-10, augment Gal-1 expression and enhance DC tolerogenicity (25). Because *T. cruzi* Tp can reprogram DCs to become tolerogenic through mechanisms that are still poorly understood (10, 16, 17), we explored whether limited anti-parasite responses in WT mice could arise from Gal-1–mediated impairment of DC immunogenicity and function. Binding of Tp to BMDCs led to considerable upregulation of Gal-1 protein expression (Fig. 5A). As compared with BMDCs from *Lgals1*$^{-/-}$ mice, *T. cruzi*–stimulated WT BMDCs ($BMDCs_{Tp}$) displayed lower MHC II expression (Fig. 5B). Moreover, LPS-stimulated WT BMDCs cultured in the presence of Tp ($BMDCs_{Tp+LPS}$) showed poorer allostimulatory capacity in MLRs compared with *Lgals1*$^{-/-}$ counterparts (Fig. 5C). Of note, T cell priming with *Lgals1*$^{-/-}$ $BMDCs_{Tp+LPS}$ resulted in augmented T cell proliferation and enhanced IL-2 and IFN-γ production compared with T cells exposed to WT $BMDCs_{Tp+LPS}$ (Fig. 5C, 5E), suggesting that *T. cruzi* subverts BMDCs immunogenicity via Gal-1–depen-

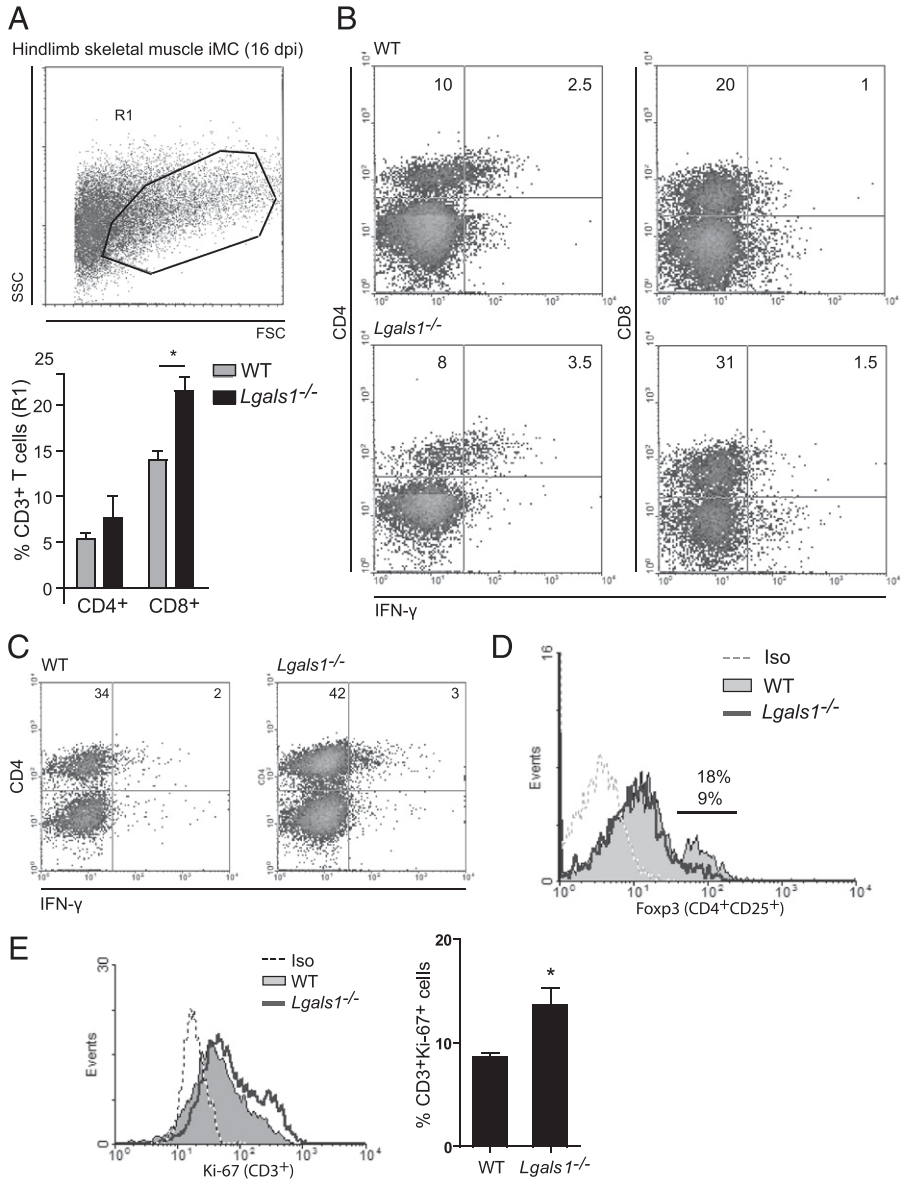

FIGURE 4. Gal-1 influences $CD4^+$ and $CD8^+$ T cell responses during the acute phase of *T. cruzi* infection. (**A**) Infiltrating mononuclear cells (iMC) obtained from hindlimb skeletal muscle tissues of WT and $Lgals1^{-/-}$ animals at 16 dpi were stained and analyzed by flow cytometry (R1 gated population, *upper panel*). The frequency of $CD4^+$ and $CD8^+$ T cells was expressed as mean ± SEM of three independent experiments performed with samples pooled from four to five mice per experimental group (*lower panel*). *$p < 0.01$, unpaired Student *t* test. (**B**) Intracytoplasmic staining of IFN-γ in infiltrating $CD4^+$ and $CD8^+$ T cells by flow cytometry. Mononuclear cells obtained from hearts isolated from WT or $Lgals1^{-/-}$ mice at 16 dpi were cultured in the presence of *T.cruzi* Ag (20 μg/ml) and brefeldin A (10 μg/ml) for 5 h at 37°C and then stained as described in *Materials and Methods*. Dot plots are representative of two independent experiments ($n = 5$/group). (**C**) Intracytoplasmic staining of IFN-γ in $CD4^+$ T cells obtained from dLNs (popliteal) at 16 dpi. Dot plots are representative of three independent experiments ($n = 2$/group). (**D**) Detection of $CD4^+CD25^+Foxp3^+$ Treg cells by flow cytometry in dLNs at 16 dpi. A representative experiment of three is shown ($n = 2$/group). Dotted line corresponds to isotype-matched control Ab, the thick line shows $Lgals1^{-/-}$ cells, and the gray histogram shows WT cells. (**E**) Intracellular detection of Ki-67 in T cells obtained from dLNs by flow cytometry at 16 dpi. One representative experiment out of three is shown (*left panel*). Dotted line corresponds to isotype-matched control Ab, the thick line shows cells from $Lgals1^{-/-}$ mice, and the gray histogram shows cells from WT mice. Graph summary (*right panel*) is expressed as mean ± SEM of three independent experiments. *$p < 0.05$, unpaired Student *t* test.

dent mechanisms. Interestingly, diminished T cell responsiveness relied not only on Tp-conditioned Gal-1–sufficient tolerogenic DCs, but also on the presence of Gal-1–sufficient T cells (Fig. 5D), suggesting that Gal-1 synthesized by both DCs and T cells contribute to parasite-induced tolerogenic circuits.

To further understand the mechanisms underlying this immunosuppressive pathway, we then examined whether Gal-1 binds to Tp. Recombinant Gal-1 bound weakly to Tp (Supplemental Fig. 2A) and neither its supplementation in cell cultures nor its endogenous deletion altered Tp binding to BMDCs or Tp infective capacity (Supplemental Fig. 2B, 2C). Interestingly, we found a trend (not statistically significant) toward increased IL-27 production in WT compared with $Lgals1^{-/-}$ BMDCs exposed to *T. cruzi* (Supplemental Fig. 2D). Accordingly, Ab-mediated blockade of IL-27p28 or IL-10 partially prevented suppression of T cell responses induced by Tp-stimulated Gal-1–sufficient WT BMDCs (Fig. 5F).

To determine whether allogeneic T cells become regulatory upon exposure to tolerogenic $BMDCs_{Tp+LPS}$, we purified $CD4^+$ T cells from a primary MLR and cultured them in a secondary

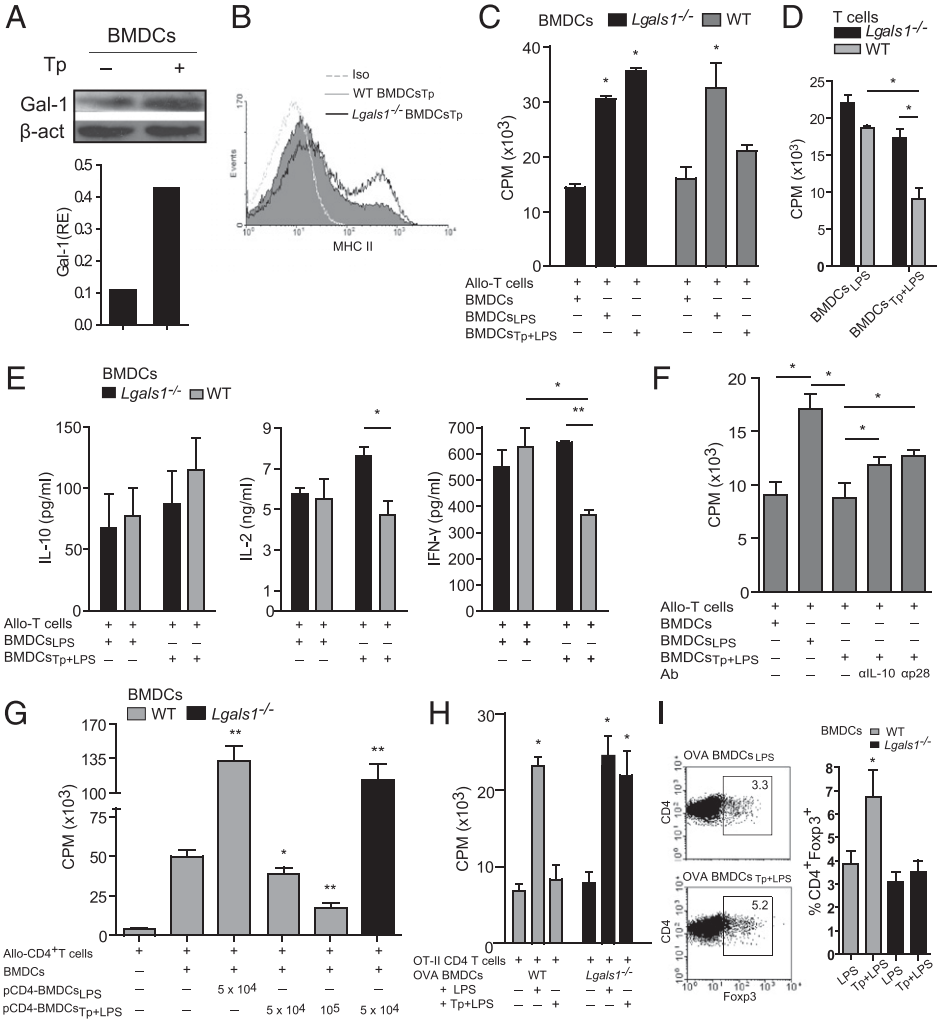

FIGURE 5. *T. cruzi* instructs DCs and T cells to become regulatory via Gal-1–dependent mechanisms. (**A**–**I**) WT or Gal-1–deficient BMDCs were stimulated for 18 h with Tp in the presence or absence of LPS and their activation status, phenotype, and allostimulatory activity were studied in vitro. (A) Immunoblot analysis of Gal-1 expression in WT BMDCs stimulated or not with Tp ($BMDCs_{Tp}$). One representative experiment of five is shown; band intensity is relative to that of β-actin (RE). (B) Flow cytometry of MHC II expression in WT or *Lgals1*$^{-/-}$ BMDCs. Open histogram shows *Lgals1*$^{-/-}$ $BMDCs_{Tp}$, gray histogram shows WT $BMDCs_{Tp}$ and dotted line shows staining with isotype-matched control Ab. One of three independent experiments is shown. (C–F) Depending on the experiment, WT or *Lgals1*$^{-/-}$ allogeneic T cells ($CD3^+$) were cocultured for 3 d with WT or *Lgals1*$^{-/-}$ BMDCs prestimulated with LPS in the absence ($BMDCs_{LPS}$) or presence ($BMDCs_{Tp+LPS}$) of Tp or left untreated (control). (C) T cell proliferation was assessed by [^{3}H]thymidine incorporation and expressed as cpm (mean ± SEM of triplicate samples). One of five representative experiments is shown. *$p < 0.05$ versus BMDC untreated controls (one-way ANOVA and Tukey posttest). (D) Influence of T cell–derived Gal-1 on DC-mediated inhibition of T cell responses. Purified $CD3^+$ T cells from WT or *Lgals1*$^{-/-}$ mice were cocultured with WT $BMDCs_{LPS}$ or $BMDCs_{Tp+LPS}$. One of five representative experiments is shown. *$p < 0.01$, two-way ANOVA and Bonferroni posttest. (E) Following cocultures described in (C), supernatants were harvested and the concentrations of IL-10, IL-2, and IFN-γ were measured by ELISA. Results are expressed as the mean ± SEM of five independent experiments. *$p < 0.05$, **$p < 0.01$ (two-way ANOVA and Bonferroni posttest). (F) [^{3}H]thymidine incorporation by allogeneic T cells cultured with WT BMDCs exposed to different stimuli in the presence or absence of IL-10 or IL-27 (p28) blocking Ab. *$p < 0.05$ (one-way ANOVA and Tukey correction). (G) Secondary MLR. Naive $CD4^+$ T cells purified from lymph nodes were primed with WT $BMDCs_{LPS}$ (pCD4-$BMDCs_{LPS}$), WT $BMDCs_{Tp+LPS}$ (pCD4-$BMDCs_{Tp+LPS}$), or *Lgals1*$^{-/-}$ $BMDCs_{Tp+LPS}$ in primary MLR. After 5 d, primed $CD4^+$ T cells ($pCD4^+$) were purified by cell sorting ($CD3^+$) and added to a secondary MLR in the presence of control BMDCs plus naive $CD4^+$ T cells. After 3 d, proliferation was assessed by [^{3}H]thymidine incorporation (mean ± SEM from triplicates). Data from one of three experiments are shown. *$p < 0.05$, **$p < 0.01$ versus allo-$CD4^+$ T cells plus BMDCs (one-way ANOVA and Tukey correction). (H and I) OVA-specific T cell response and differentiation assay after OT-II $CD4^+$ T cell culture with WT or *Lgals1*$^{-/-}$ BMDCs exposed to different stimuli and OVA peptide (50 μg/ml) as described in *Materials and Methods*. (H) Proliferation of OVA-specific OT-II $CD4^+$ T cells was measured by [^{3}H]thymidine incorporation. Results are expressed as mean ± SEM from triplicates ($n = 3$). *$p < 0.05$ versus BMDCs untreated control (one-way ANOVA, Tukey posttest). (I) Analysis of $CD4^+Foxp3^+$ T cells by flow cytometry after culturing purified OVA-specific naive $CD4^+CD62L^{high}$ T cells as described in *Materials and Methods*. Dot plots representative of three independent experiments are shown (*left*). Summary bars (*right*) are expressed as the mean ± SEM ($n = 3$). *$p < 0.05$, unpaired Student *t* test.

MLR. We found dose-dependent inhibition of $CD4^+$ T cell proliferation when these cells were cocultured with $CD4^+$ T cells primed with WT but not with Gal-1–deficient $BMDCs_{Tp+LPS}$ (Fig. 5G). Because Gal-1 controls the suppressive activity of Treg cells (43), we then examined whether tolerogenic $BMDCs_{Tp+LPS}$ induced the differentiation of Treg cells in vitro by analyzing OVA-specific T cell responses. We found inhibition of OVA-specific T cell proliferation and induction of $CD4^+Foxp3^+$ Treg cells after coculturing naive $CD4^+CD62L^{high}$ T cells purified from OT-II mice with OVA-pulsed syngeneic WT but not *Lgals1*$^{-/-}$

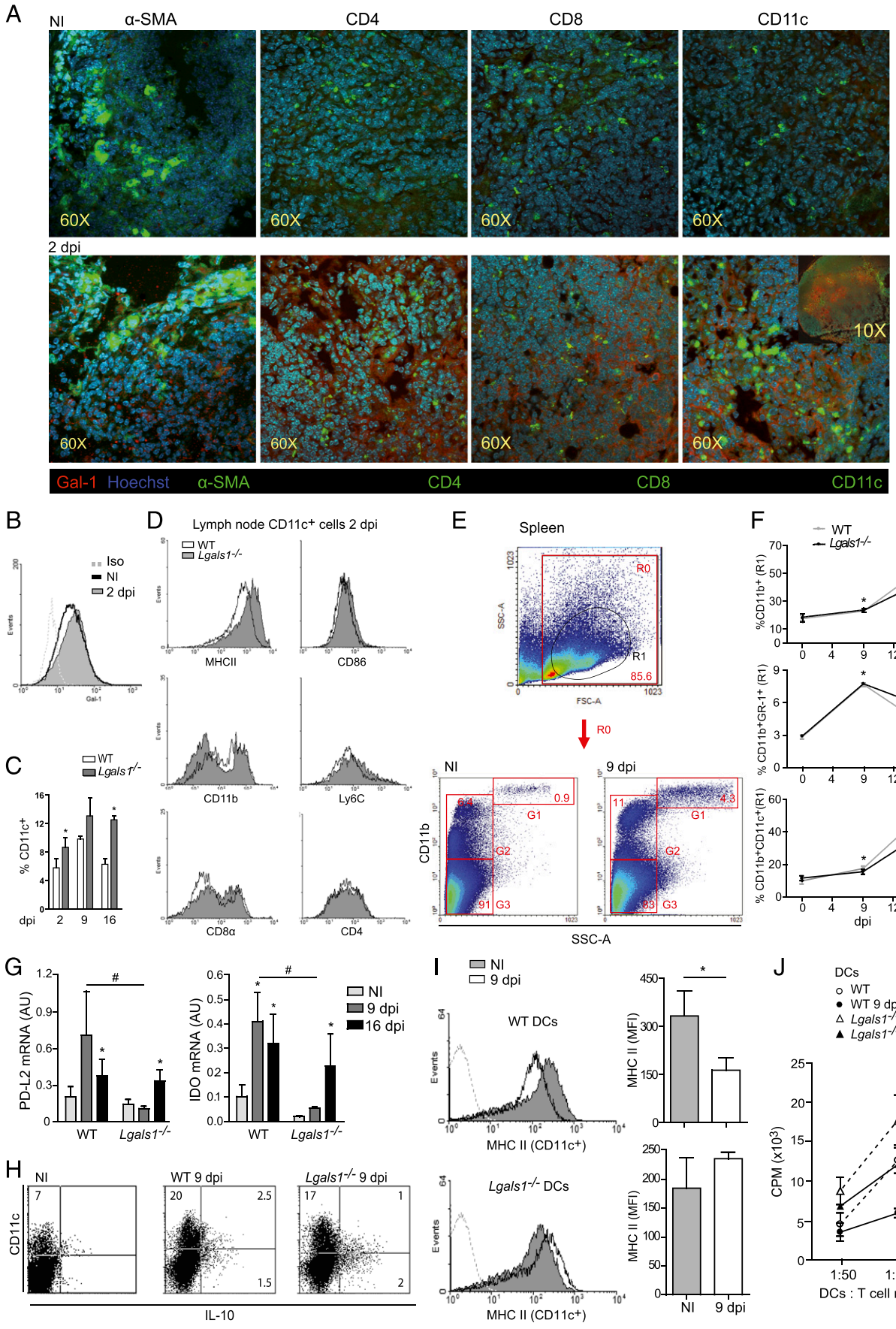

FIGURE 6. *T. cruzi*–driven tolerogenic circuits are mediated by endogenous Gal-1 in vivo. dLNs (popliteal) or spleens were obtained from WT and/or *Lgals1*$^{-/-}$ mice 2, 9, or 16 dpi depending on the assay. (**A** and **B**) Expression of Gal-1 in dLNs from noninfected (NI) or infected (2 dpi) WT mice. (A) Confocal microscopy analysis. Sections were stained with Hoechst 33258 for nuclei (blue), anti–Gal-1 Ab (red), and Ab against (*Figure legend continues*)

$BMDCs_{Tp+LPS}$ (Fig. 5H, 5I). Thus, Gal-1–sufficient DCs respond to Tp by acquiring tolerogenic properties that influence the differentiation of fully functional suppressive Treg cells.

Exposure to Gal-1 endows DCs with tolerogenic potential during acute T. cruzi *infection*

Previous reports documented the presence of myeloid regulatory cells in the spleen of *T. cruzi*–infected mice that counteract parasite-induced exacerbation of inflammatory responses (45–47). In this regard, we and others have demonstrated that APCs, including DCs, display altered maturation during experimental *T. cruzi* infection (10, 12). In this study, we detected high expression of Gal-1 in dLNs early during infection (2 dpi) in the vicinity of $CD11c^+$ DC areas (Fig. 6A). Intracellular flow cytometry confirmed upregulated expression of Gal-1 at 2 dpi (Fig. 6B). To explore how Gal-1 deficiency influences the generation of immunogenic DCs in vivo, we first examined the presence of different cell populations in dLNs and spleens from *Lgals1*$^{-/-}$ and WT infected mice. Interestingly, we detected a time-dependent influx of $CD11c^+$ DCs to dLNs that was more pronounced in *Lgals1*$^{-/-}$ mice than in WT infected animals at 2 and 16 dpi (Fig. 6C). Whereas no substantial differences were observed in the type of DC populations recruited to lymph nodes of WT and *Lgals1*$^{-/-}$ mice, $CD11c^+$ DCs from *Lgals1*$^{-/-}$ mice expressed higher expression of MHC II than did their WT counterpart (Fig. 6D). Thus, DCs lacking Gal-1 are equipped with greater T cell stimulatory capacity in response to *T. cruzi* infection in vivo.

Interestingly, and regardless of Gal-1 expression, spleen enlargement in *T. cruzi*–infected mice was associated with the recruitment of $CD11b^+$ myeloid cells (Fig. 6E, 6F, *upper panel*). Parasite infection enhanced both the number of $CD11b^+Gr1^+$ granulocytes (Fig. 6E, gate G1, *lower panel*, 6F, *middle panel*) and myeloid–mononuclear cells, including $CD11b^+CD11c^+$ "DC-like" cells, $CD11b^+Ly6C^{high}$ monocytes, and $F4/80^+$ macrophages (Fig. 6F, *lower panel* and data not shown). Following analysis of the R1 region (Fig. 6E, *upper panel*), we observed that both $CD11b^+Gr1^+$ and $CD11b^+CD11c^+$ populations were increased in WT and *Lgals1*$^{-/-}$-infected mice at 9 dpi; however, accumulation of DCs was greater in WT infected mice at 16 dpi (Fig. 6F, *lower panel*). The largest expansion of the myeloid cell compartment in WT-infected mice was preceded by considerable upregulation of PD-L2 and IDO mRNA (Fig. 6G) and augmented IL-10 production by $CD11c^+$ DCs (Fig. 6H), suggesting a key role of endogenous Gal-1 in activating tolerogenic pathways in vivo during *T. cruzi* infection.

To further analyze the activation status of splenic DCs, we purified $CD11c^+$ cells from WT and *Lgals1*$^{-/-}$-infected and non-infected mice and analyzed MHC II surface expression and allostimulatory capacity ex vivo. Parasite infection led to downregulation of MHC II expression in splenic DCs from WT animals (Fig. 6I). Moreover, these cells displayed diminished capacity to stimulate allogeneic T cell responses compared with splenic DCs from *Lgals1*$^{-/-}$-infected mice or DCs from noninfected WT mice (Fig. 6J). Thus, DC-derived Gal-1 is essential for activation of tolerogenic circuits and impairment of T cell responses triggered by *T. cruzi* infection in vivo.

Adoptive transfer of DCs lacking Gal-1 enhances resistance to T. cruzi *infection and stimulates T cell–dependent anti-parasite immunity*

As compared with their WT counterpart, *Lgals1*$^{-/-}$-infected mice showed higher frequency of $CD8^+$ T cells infiltrating tissues, higher responsiveness of Ag-specific $CD4^+$ T cells ex vivo, and lower numbers of $CD4^+CD25^+Foxp3^+$ Treg cells in secondary lymphoid organs together with more immunogenic DCs (Figs. 4, 5). To address the capacity of Gal-1–deficient DCs to overcome T cell unresponsiveness in vivo, we adoptively transferred DCs purified from spleens of early infected *Lgals1*$^{-/-}$ or WT mice into WT recipients prior to infection as described in *Materials and Methods*. We found that mice receiving *Lgals1*$^{-/-}$ DCs displayed lower blood parasite counts and lower susceptibility to *T. cruzi* infection compared with mice transferred with WT DCs or non-transferred WT mice (Fig. 7A, 7B). Additionally, *T. cruzi*–infected WT mice receiving *Lgals1*$^{-/-}$ DCs displayed an enhanced Th1 response at 14 dpi as shown by the greater number of IFN-γ–producing $CD4^+$ T cells in the spleen (Fig. 7C) and inguinal lymph nodes (Fig. 7D) compared with WT infected mice transferred with Gal-1–sufficient DCs. This effect was accompanied by a lower frequency of $CD4^+CD25^+Foxp3^+$ T cells in inguinal lymph nodes (Fig. 7E). Thus, disruption of Gal-1 on DCs contributes, at least in part, to thwart parasite-driven tolerogenic circuits, to amplify Th1 immunity, and to enhance resistance to *T. cruzi* infection.

All together, our results show that *T. cruzi* infection triggers a regulatory program mediated by endogenous Gal-1, which favors parasite persistence (Fig. 8).

Discussion

In the present study, we identified a regulatory circuit hierarchically driven by the endogenous β-galactoside–binding lectin Gal-1 that contributes to differentiation of tolerogenic DCs and $Foxp3^+$ Treg

α-smooth muscle actin (α-SMA), CD4, CD8, or CD11c (green) Abs as described in *Materials and Methods*. Images of individual markers were acquired with the same parameters using ×60 or ×10 original magnification. (**B**) Detection of intracellular Gal-1 by flow cytometry. One representative experiment of three is shown both in (A) and (B). (**C**) Single-cell suspensions were obtained from dLNs of WT and *Lgals1*$^{-/-}$ mice at 2, 9, and 16 dpi and the percentage of $CD11c^+$ cells was determined by flow cytometry. Mean ± SEM of three independent experiments is shown. $*p < 0.05$, unpaired Student *t* test. (**D**) Two-day postinfection single-cell suspensions from dLNs of WT and *Lgals1*$^{-/-}$ mice were analyzed by flow cytometry for the expression of CD11c. Gated $CD11c^+$ cells were further analyzed for MHC II, CD86, CD11b, Ly-6C, CD8α, and CD4 expression. One representative experiment of three is shown. (**E** and **F**) Characterization of the myeloid cell compartment in spleens of infected WT and *Lgals1*$^{-/-}$ mice isolated at 9 or 16 dpi. (E) Gating strategy for $CD11b^+$ cells. (F) Granulocytes ($CD11b^+Gr\text{-}1^+$) and myeloid DCs ($CD11b^+CD11c^+$) gated in the R1 region (E, *upper panel*) from WT and *Lgals1*$^{-/-}$ mice. Results are expressed as the mean ± SEM of five independent experiments. $*p < 0.05$, $**p < 0.01$ infected versus noninfected (NI); $^{\#}p < 0.05$ WT versus *Lgals1*$^{-/-}$ (two-way ANOVA and Bonferroni posttest). (**G**) Total RNA from splenocytes of WT and *Lgals1*$^{-/-}$ mice was obtained and PD-L2 and IDO mRNA were measured by quantitative real-time RT-PCR. Results are presented relative to GAPDH mRNA and expressed as mean ± SEM ($n = 5$/condition, three independent experiments). $*p < 0.05$ infected versus NI, $^{\#}p < 0.05$ WT versus *Lgals1*$^{-/-}$-infected mice (two-way ANOVA and Bonferroni posttest). (**H**) Splenic $CD11c^+IL\text{-}10^+$ cells were analyzed by flow cytometry at 9 dpi using R1 gating strategy. Representative dot plots of three independent experiments with similar results are shown. (**I** and **J**) $CD11c^+$ DCs were purified from the spleen of NI or infected WT and *Lgals1*$^{-/-}$ mice at 9 dpi and their activation status was determined. (I) MHC II expression analyzed by flow cytometry. MFI, mean fluorescence intensity ($n = 3$, mean ± SEM). $*p < 0.05$, unpaired Student *t* test. (J) Purified DCs were cocultured with $CD3^+$ T cells (BALB/c) and their allostimulatory capacity was analyzed ex vivo. Proliferation was assessed by $[^3H]$thymidine incorporation. One of three independent experiments is shown and represented as mean ± SEM from triplicates. $*p < 0.05$ NI WT versus WT 9 dpi and WT 9 dpi versus *Lgals1*$^{-/-}$ 9 dpi (two-way ANOVA and Bonferroni posttest).

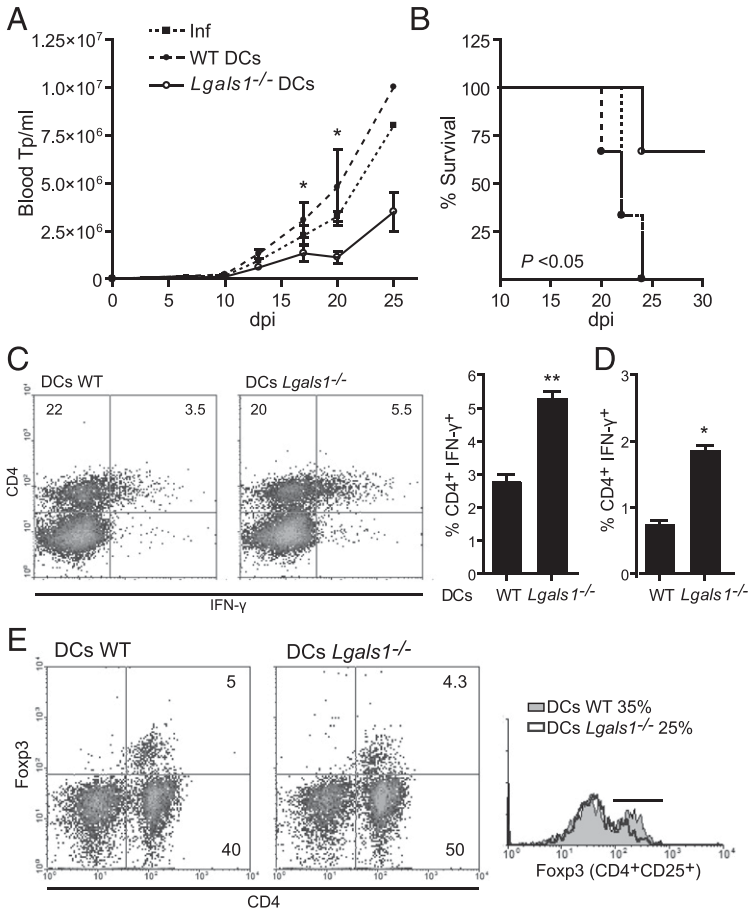

FIGURE 7. Adoptive transfer of DCs lacking Gal-1 enhances resistance to *T. cruzi* infection and stimulates T cell–dependent anti-parasite immunity. WT mice were adoptively transferred with *Lgals1*$^{-/-}$ or WT DCs (i.p.) and infected with 100 RA-Tp using the same inoculation route. Blood parasitemia (**A**) and survival curves analyzed by Kaplan–Meier (**B**) from WT infected mice receiving WT DCs (●) or *Lgals1*$^{-/-}$ DCs (○) are shown. Infected mice not receiving DCs are shown as closed squares. A representative experiment of two is shown, performed with at least three to six mice per group. Parasitemia is expressed as mean ± SEM. $*p < 0.05$, unpaired Student *t* test. (**C** and **D**) Ex vivo IFN-γ production by CD4$^+$ T cells isolated from spleen (C) or dLNs (D) from *T. cruzi*–infected mice receiving *Lgals1*$^{-/-}$ or WT DCs. Intracellular IFN-γ was detected by flow cytometry after stimulation with *T. cruzi* Ag (20 μg/ml) in vitro. Dot plots of two independent experiments are shown ($n = 2$). Results are expressed as mean ± SEM. $*p < 0.05$, $**p < 0.01$, unpaired Student *t* test. (**E**) Flow cytometry of CD4$^+$Foxp3$^+$ T cells (dot plot) or Foxp3$^+$ cells in CD4$^+$CD25$^+$ gated population (histogram) from inguinal lymph nodes isolated at 14 dpi from infected WT mice receiving *Lgals1*$^{-/-}$ or WT DCs. One of two independent experiments with similar results is shown ($n = 2$ animals/group).

cells during acute *T. cruzi* infection, blunts effector T cell responses, and favors parasite persistence in host tissues (Fig. 8). Although susceptibility to acute *T. cruzi* infection relies on the inoculum, the route of parasite entrance, and the strains of mice and parasites, pathogenesis is associated with a Th1-type inflammatory process that not only controls parasite burden, but can also damage host tissue (4, 8, 48). As a result, the outcome of infection and host survival depends both on the preservation of tissue integrity and parasite elimination.

Despite the ability of effector T cells to limit *T. cruzi* spreading (8, 9), the parasite cannot be completely cleared, suggesting the activation of multiple immune evasion strategies and tolerogenic circuits, which negatively regulate anti-parasite responses (6, 11, 16). Accordingly, components from the surface of Tp were found to shape DC tolerogenicity via pattern recognition receptors (17). Additionally, recent findings demonstrated that *T. cruzi* strains belonging to different discrete typing units display distinct strategies for immune evasion, leading to negative modulation of DC

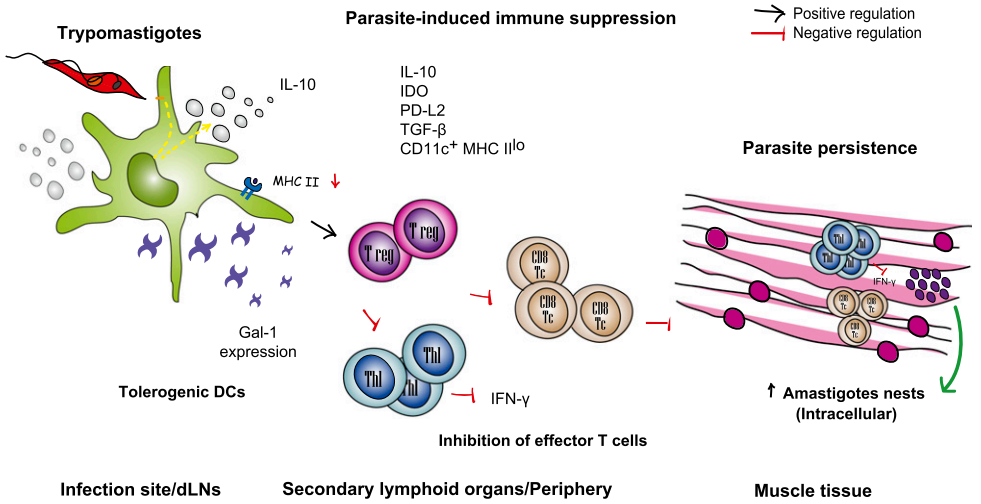

FIGURE 8. Schematic representation of the Gal-1–mediated regulatory circuit triggered during acute *T. cruzi* infection. Early after parasite entry, *T. cruzi* Tp foster a tolerogenic circuit involving the release of anti-inflammatory mediators by DCs, downregulation of MHC II expression, induction of CD4$^+$ Foxp3$^+$ Treg cells, and inhibition of effector Th1 and CD8$^+$ T cell responses. This regulatory network leads to increased parasite burden in muscle tissues and greater susceptibility to infection. Tc, cytotoxic T cells.

physiology (49). Results shown in the present study demonstrate that *T. cruzi* usurps the Gal-1 pathway to impart a tolerogenic program mediated by DCs and T cells early after infection.

Lectin–glycan interactions critically influence immune tolerance and homeostasis by selectively dampening pathogenic T cell responses, by instructing the differentiation of tolerogenic DCs, and/or by promoting differentiation, expansion, and/or recruitment of Treg cells (19). Lectin–glycan lattices can also control host–pathogen interactions by acting as pattern recognition receptors that trigger a variety of signaling pathways to amplify or resolve parasite-associated inflammatory responses (26, 27). Gal-1 binds to glycans on a variety of viral envelope glycoproteins, controlling viral adsorption and infection of target cells (22, 23). In this context, recent findings indicated the ability of this endogenous lectin to enhance the binding of the protozoan parasite *Trichomonas vaginalis* to cervical epithelial cells (34), whereas Gal-3 and Gal-9 can bind glycan structures in trypanosomatids (28, 33). Regarding *T. cruzi*, Pineda et al. (39) recently showed the differential recognition of 14 different strains of *T. cruzi* corresponding to variable genetic lineages by human Gal-1, -3, -4, -7, and -8. In the present study, we observed substantial upregulation of Gal-1 in *T. cruzi*–infected mice and higher parasite load in skeletal muscle and heart from WT infected versus *Lgals1*$^{-/-}$ mice. However, we found no direct correlation between Gal-1 expression and *T. cruzi* invasion of myeloid host cells. Although Gal-1 bound weakly to Tp, no biological effect could be associated to this interaction under our experimental conditions, as neither exogenous nor endogenous Gal-1 could influence parasite access to myeloid cells in culture. Moreover, we recently found that both exogenous and endogenous Gal-1 inhibit infection of cardiac cells in a carbohydrate-dependent fashion (A.F. Benatar, G.A. Garcia, J. Buá, J.P. Cerliani, M. Postan, L.M. Tasso, J. Scaglione, J.C. Stupirski, M.A. Toscano, G.A. Rabinovich, K.A. Gómez, unpublished data). These results rule out a possible role of Gal-1 as a positive mediator of muscle parasitism and reinforce the notion that Gal-1 acts mainly by dampening anti-parasite immunity.

In cancer and autoimmune settings, Gal-1 has been implicated in the control of tolerogenic programs by modulating tumor cell evasion of immune responses and promoting the resolution of chronic inflammatory responses (24). Nevertheless, the role of this lectin in regulating anti-parasite immunity in vivo has not yet been examined. Previous studies demonstrated the expression of Gal-1 in *T. cruzi*–infected immune cells (35, 36). Moreover, in human settings, this lectin has been shown to be prominently expressed in cardiac tissue from patients with severe chronic Chagas' disease (50). In this study, we demonstrate a tolerogenic role for Gal-1 during acute *T. cruzi* infection. Two days after the parasite entry, dLNs showed augmented expression of Gal-1, which critically influenced the tolerogenic properties of DCs and T cells, leading to parasite persistence through downmodulation of Th1 responses. Infected WT mice Gal-1–deficient DCs showed greater frequency of IFN-γ–producing CD4$^+$ T cells, displayed lower number of Foxp3$^+$ Treg cells in dLNs, and developed augmented Th1 responses in peripheral tissues.

CD8$^+$ T cells are considered to be key contributors to Chagas' disease–associated cardiomyopathy (7, 8), and mice survival is linked to low parasitemia and high frequency of IFN-γ/IL-10 double-positive CD8 effector T cells in the myocardium (51). Several regulatory pathways have been shown to contribute to inhibition of both CD8$^+$ and Th1-type responses (9). It has become clear that distinct DC subpopulations may exhibit divergent functions in vivo either evoking inflammatory responses or favoring immune tolerance during the course of parasite infection. These cells may activate tolerogenic programs through promotion of T cell anergy or induction of Treg cells (52, 53). Inducible Treg cells may play a paradoxical role in defining the outcome of infectious diseases, as they may prevent pathogen clearance or limit collateral tissue damage through suppression of inflammatory responses (54–56). Interestingly, in a model of murine cerebral malaria, removal of Treg cells reduced parasite spreading and attenuated the pathogenic process in the brain (57). However, during *T. cruzi* infection, depletion of Treg cells led to contradictory results, although an overall analysis of these studies revealed a dominant role for these cells in controlling parasite elimination (58–60). Contrasting results could be due to the use of different strategies leading to Treg cell depletion or to inhibition of clonal expansion of activated T cells through CD25 blockade. Moreover, during parasite infections, suppressive mechanisms and immune evasive programs may vary according to pathogen-intrinsic characteristics, their entry route, stage of infection, and different molecules involved in pathogen recognition (54). In this context, Gal-1 could play a pivotal role by hierarchically regulating tolerogenic programs at different stages of the disease (19). During the acute stage of the disease, *T. cruzi* may condition DCs to produce high amounts of Gal-1, which together with IL-10 and TGF-β_1 (16) may influence the course of Chagas' disease. Further studies are warranted to elucidate the DC receptors and signaling pathways implicated in *T. cruzi*–induced Gal-1 synthesis.

Assessment of specific and effective anti-parasite responses in Chagas' disease has become complex because acute *T. cruzi* infection is followed by extensive polyclonal activation even before the immune system mounts particular T cell responses (8, 9). In this study, we identified augmented Th1 cells associated with low parasite burden in secondary lymphoid organs and tissues from *Lgals1*$^{-/-}$-infected mice or in WT mice adoptively transferred with Gal-1–deficient DCs, suggesting that interruption of the Gal-1–glycan axis may contribute to circumvent parasite-driven tolerogenic pathways.

Genetic classification of *T. cruzi* strains constitutes a framework to study the biological variability linked to parasite pathogenicity. Intrinsic characteristics of this pathogen such as virulence factors, Ag composition, and tissue tropism may affect the outcome of infection. Monteiro et al. (61) have previously described the effect of cruzipain, a parasite cysteine protease, in the release of endogenous mediators sensed by bradykinin B_2 receptor in cooperation with TLR2 for the induction of Th1-dependent immunity. The authors further showed the critical role of B_2 receptor in promoting DC activation and evoking protective responses in response to kinins proteolytically released by the parasite (62). Whether engagement of TLR2 or the B_2 receptor on DCs may influence the Gal-1 tolerogenic pathway still remains to be elucidated. Additionally, given the involvement of TLR4 in IL-10 induction during *T. cruzi*–BMDC interaction (17), further studies are required to investigate the possible interplay between TLR4 and the Gal-1 tolerogenic pathway during parasite infection. Interestingly, *T. cruzi* may display diverse Ag composition and variable enzymatic activities, depending on parasite strains. In this regard, previous work has described stage dependency in cruzipain expression in RA (63) and higher representation of *trans*-sialidase in more virulent strains (64). Emerging evidence also demonstrates that individual strains can elicit different proinflammatory responses through mechanisms involving GPI-associated mucins (65). Thus, low expression of danger signals such as GPI-associated mucins, cruzipain, and/or *trans*-sialidase may explain preferential reprograming of DC phenotype by different strains (49) and subsequent regulation of anti-parasite immunity.

In summary, in this study, we identified a critical role for endogenous Gal-1 in modulating the outcome of *T. cruzi* infection

by fueling immunosuppressive circuits, involving tolerogenic DCs and Tregs, that contribute to dampen anti-parasite immunity. A more complete understanding of the immunoevasive programs elicited by *T. cruzi* will contribute to the design of rational strategies for the control of Chagas' disease.

Acknowledgments

We thank S. Dergan Dylon, D. Croci, N. Macchiaroli, and W. Unger for advice and E. Gimenez, S. Gatto, and R. Morales for technical assistance.

Disclosures

The authors have no financial conflicts of interest.

References

1. World Health Organization. 2010. Chagas disease: control and elimination. Available at: http://apps.who.int/gb/ebwha/pdf_files/WHA63/A63_17-en.pdf.
2. Marin-Neto, J. A., E. Cunha-Neto, B. C. Maciel, and M. V. Simões. 2007. Pathogenesis of chronic Chagas heart disease. *Circulation* 115: 1109–1123.
3. Abrahamsohn, I. A. 1998. Cytokines in innate and acquired immunity to *Trypanosoma cruzi* infection. *Braz. J. Med. Biol. Res.* 31: 117–121.
4. da Matta Guedes, P. M., F. R. Gutierrez, F. L. Maia, C. M. Milanezi, G. K. Silva, W. R. Pavanelli, and J. S. Silva. 2010. IL-17 produced during *Trypanosoma cruzi* infection plays a central role in regulating parasite-induced myocarditis. *PLoS Negl. Trop. Dis.* 4: e604.
5. Tarleton, R. L., M. J. Grusby, M. Postan, and L. H. Glimcher. 1996. *Trypanosoma cruzi* infection in MHC-deficient mice: further evidence for the role of both class I- and class II-restricted T cells in immune resistance and disease. *Int. Immunol.* 8: 13–22.
6. Martin, D. L., D. B. Weatherly, S. A. Laucella, M. A. Cabinian, M. T. Crim, S. Sullivan, M. Heiges, S. H. Craven, C. S. Rosenberg, M. H. Collins, et al. 2006. $CD8^+$ T-cell responses to *Trypanosoma cruzi* are highly focused on strain-variant *trans*-sialidase epitopes. *PLoS Pathog.* 2: e77.
7. Rosenberg, C. S., D. L. Martin, and R. L. Tarleton. 2010. $CD8^+$ T cells specific for immunodominant trans-sialidase epitopes contribute to control of *Trypanosoma cruzi* infection but are not required for resistance. *J. Immunol.* 185: 560–568.
8. Teixeira, M. M., R. T. Gazzinelli, and J. S. Silva. 2002. Chemokines, inflammation and *Trypanosoma cruzi* infection. *Trends Parasitol.* 18: 262–265.
9. DosReis, G. A. 2011. Evasion of immune responses by *Trypanosoma cruzi*, the etiological agent of Chagas disease. *Braz. J. Med. Biol. Res.* 44: 84–90.
10. Van Overtvelt, L., M. Andrieu, V. Verhasselt, F. Connan, J. Choppin, V. Vercruysse, M. Goldman, A. Hosmalin, and B. Vray. 2002. *Trypanosoma cruzi* down-regulates lipopolysaccharide-induced MHC class I on human dendritic cells and impairs antigen presentation to specific $CD8^+$ T lymphocytes. *Int. Immunol.* 14: 1135–1144.
11. Planelles, L., M. C. Thomas, C. Marañón, M. Morell, and M. C. López. 2003. Differential CD86 and CD40 co-stimulatory molecules and cytokine expression pattern induced by *Trypanosoma cruzi* in APCs from resistant or susceptible mice. *Clin. Exp. Immunol.* 131: 41–47.
12. Alba Soto, C. D., G. A. Mirkin, M. E. Solana, and S. M. González Cappa. 2003. *Trypanosoma cruzi* infection modulates in vivo expression of major histocompatibility complex class II molecules on antigen-presenting cells and T-cell stimulatory activity of dendritic cells in a strain-dependent manner. *Infect. Immun.* 71: 1194–1199.
13. Steinman, R. M., D. Hawiger, and M. C. Nussenzweig. 2003. Tolerogenic dendritic cells. *Annu. Rev. Immunol.* 21: 685–711.
14. Hammer, G. E., and A. Ma. 2013. Molecular control of steady-state dendritic cell maturation and immune homeostasis. *Annu. Rev. Immunol.* 31: 743–791.
15. Van Overtvelt, L., N. Vanderheyde, V. Verhasselt, J. Ismaili, L. De Vos, M. Goldman, F. Willems, and B. Vray. 1999. *Trypanosoma cruzi* infects human dendritic cells and prevents their maturation: inhibition of cytokines, HLA-DR, and costimulatory molecules. *Infect. Immun.* 67: 4033–4040.
16. Poncini, C. V., C. D. Alba Soto, E. Batalla, M. E. Solana, and S. M. González Cappa. 2008. *Trypanosoma cruzi* induces regulatory dendritic cells in vitro. *Infect. Immun.* 76: 2633–2641.
17. Poncini, C. V., G. Giménez, C. A. Pontillo, C. D. Alba-Soto, E. L. de Isola, I. Piazzón, and S. M. Cappa. 2010. Central role of extracellular signal-regulated kinase and Toll-like receptor 4 in IL-10 production in regulatory dendritic cells induced by *Trypanosoma cruzi*. *Mol. Immunol.* 47: 1981–1988.
18. van Kooyk, Y., and G. A. Rabinovich. 2008. Protein-glycan interactions in the control of innate and adaptive immune responses. *Nat. Immunol.* 9: 593–601.
19. Rabinovich, G. A., and M. A. Toscano. 2009. Turning "sweet" on immunity: galectin-glycan interactions in immune tolerance and inflammation. *Nat. Rev. Immunol.* 9: 338–352.
20. Toscano, M. A., G. A. Bianco, J. M. Ilarregui, D. O. Croci, J. Correale, J. D. Hernandez, N. W. Zwirner, F. Poirier, E. M. Riley, L. G. Baum, and G. A. Rabinovich. 2007. Differential glycosylation of T_H1, T_H2 and T_H-17 effector cells selectively regulates susceptibility to cell death. *Nat. Immunol.* 8: 825–834.
21. Toscano, M. A., A. G. Commodaro, J. M. Ilarregui, G. A. Bianco, A. Liberman, H. M. Serra, J. Hirabayashi, L. V. Rizzo, and G. A. Rabinovich. 2006. Galectin-1 suppresses autoimmune retinal disease by promoting concomitant Th2- and T regulatory-mediated anti-inflammatory responses. *J. Immunol.* 176: 6323–6332.
22. Levroney, E. L., H. C. Aguilar, J. A. Fulcher, L. Kohatsu, K. E. Pace, M. Pang, K. B. Gurney, L. G. Baum, and B. Lee. 2005. Novel innate immune functions for galectin-1: galectin-1 inhibits cell fusion by Nipah virus envelope glycoproteins and augments dendritic cell secretion of proinflammatory cytokines. *J. Immunol.* 175: 413–420.
23. Ouellet, M., S. Mercier, I. Pelletier, S. Bounou, J. Roy, J. Hirabayashi, S. Sato, and M. J. Tremblay. 2005. Galectin-1 acts as a soluble host factor that promotes HIV-1 infectivity through stabilization of virus attachment to host cells. *J. Immunol.* 174: 4120–4126.
24. Rabinovich, G. A., and D. O. Croci. 2012. Regulatory circuits mediated by lectin-glycan interactions in autoimmunity and cancer. *Immunity* 36: 322–335.
25. Ilarregui, J. M., D. O. Croci, G. A. Bianco, M. A. Toscano, M. Salatino, M. E. Vermeulen, J. R. Geffner, and G. A. Rabinovich. 2009. Tolerogenic signals delivered by dendritic cells to T cells through a galectin-1-driven immunoregulatory circuit involving interleukin 27 and interleukin 10. *Nat. Immunol.* 10: 981–991.
26. Vasta, G. R. 2009. Roles of galectins in infection. *Nat. Rev. Microbiol.* 7: 424–438.
27. Baum, L. G., O. B. Garner, K. Schaefer, and B. Lee. 2014. Microbe-host interactions are positively and negatively regulated by galectin-glycan interactions. *Front. Immunol.* 5: 284.
28. Pelletier, I., and S. Sato. 2002. Specific recognition and cleavage of galectin-3 by *Leishmania major* through species-specific polygalactose epitope. *J. Biol. Chem.* 277: 17663–17670.
29. Kohatsu, L., D. K. Hsu, A. G. Jegalian, F. T. Liu, and L. G. Baum. 2006. Galectin-3 induces death of Candida species expressing specific β-1,2-linked mannans. *J. Immunol.* 177: 4718–4726.
30. Stowell, S. R., C. M. Arthur, M. Dias-Baruffi, L. C. Rodrigues, J. P. Gourdine, J. Heimburg-Molinaro, T. Ju, R. J. Molinaro, C. Rivera-Marrero, B. Xia, et al. 2010. Innate immune lectins kill bacteria expressing blood group antigen. *Nat. Med.* 16: 295–301.
31. Garner, O. B., H. C. Aguilar, J. A. Fulcher, E. L. Levroney, R. Harrison, L. Wright, L. R. Robinson, V. Aspericueta, M. Panico, S. M. Haslam, et al. 2010. Endothelial galectin-1 binds to specific glycans on nipah virus fusion protein and inhibits maturation, mobility, and function to block syncytia formation. *PLoS Pathog.* 6: e1000993.
32. Toledo, K. A., M. L. Fermino, Cdel. C. Andrade, T. B. Riul, R. T. Alves, V. D. Muller, R. R. Russo, S. R. Stowell, R. D. Cummings, V. H. Aquino, and M. Dias-Baruffi. 2014. Galectin-1 exerts inhibitory effects during DENV-1 infection. *PLoS One* 9: e112474.
33. Kleshchenko, Y. Y., T. N. Moody, V. A. Furtak, J. Ochieng, M. F. Lima, and F. Villalta. 2004. Human galectin-3 promotes *Trypanosoma cruzi* adhesion to human coronary artery smooth muscle cells. *Infect. Immun.* 72: 6717–6721.
34. Okumura, C. Y., L. G. Baum, and P. J. Johnson. 2008. Galectin-1 on cervical epithelial cells is a receptor for the sexually transmitted human parasite *Trichomonas vaginalis*. *Cell. Microbiol.* 10: 2078–2090.
35. Zuñiga, E., G. A. Rabinovich, M. M. Iglesias, and A. Gruppi. 2001. Regulated expression of galectin-1 during B-cell activation and implications for T-cell apoptosis. *J. Leukoc. Biol.* 70: 73–79.
36. Zúñiga, E., A. Gruppi, J. Hirabayashi, K. I. Kasai, and G. A. Rabinovich. 2001. Regulated expression and effect of galectin-1 on *Trypanosoma cruzi*-infected macrophages: modulation of microbicidal activity and survival. *Infect. Immun.* 69: 6804–6812.
37. Vray, B., I. Camby, V. Vercruysse, T. Mijatovic, N. V. Bovin, P. Ricciardi-Castagnoli, H. Kaltner, I. Salmon, H. J. Gabius, and R. Kiss. 2004. Up-regulation of galectin-3 and its ligands by *Trypanosoma cruzi* infection with modulation of adhesion and migration of murine dendritic cells. *Glycobiology* 14: 647–657.
38. Ferrer, M. F., C. A. Pascuale, R. M. Gomez, and M. S. Leguizamón. 2014. DTU I isolates of *Trypanosoma cruzi* induce upregulation of galectin-3 in murine myocarditis and fibrosis. *Parasitology* 141: 849–858.
39. Pineda, M. A., L. Corvo, M. Soto, M. Fresno, and P. Bonay. 2015. Interactions of human galectins with *Trypanosoma cruzi*: binding profile correlate with genetic clustering of lineages. *Glycobiology* 25: 197–210.
40. González Cappa, S. M., A. T. Bijovsky, H. Freilij, L. Muller, and A. M. Katzin. 1981. [Isolation of a *Trypanosoma cruzi* strain of predominantly slender form in Argentina]. *Medicina (B. Aires)* 41: 119–120.
41. Zingales, B., S. G. Andrade, M. R. Briones, D. A. Campbell, E. Chiari, O. Fernandes, F. Guhl, E. Lages-Silva, A. M. Macedo, C. R. Machado, et al; Second Satellite Meeting. 2009. A new consensus for *Trypanosoma cruzi* intraspecific nomenclature: second revision meeting recommends TcI to TcVI. *Mem. Inst. Oswaldo Cruz* 104: 1051–1054.
42. Solana, M. E., C. D. Alba Soto, M. C. Fernández, C. V. Poncini, M. Postan, and S. M. González Cappa. 2009. Reduction of parasite levels in blood improves pregnancy outcome during experimental *Trypanosoma cruzi* infection. *Parasitology* 136: 627–639.
43. Garín, M. I., C. C. Chu, D. Golshayan, E. Cernuda-Morollón, R. Wait, and R. I. Lechler. 2007. Galectin-1: a key effector of regulation mediated by $CD4^+$ $CD25^+$ T cells. *Blood* 109: 2058–2065.
44. Cedeno-Laurent, F., M. Opperman, S. R. Barthel, V. K. Kuchroo, and C. J. Dimitroff. 2012. Galectin-1 triggers an immunoregulatory signature in Th cells functionally defined by IL-10 expression. *J. Immunol.* 188: 3127–3137.
45. Goñi, O., P. Alcaide, and M. Fresno. 2002. Immunosuppression during acute *Trypanosoma cruzi* infection: involvement of Ly6G $(Gr1^+)CD11b^+$ immature myeloid suppressor cells. *Int. Immunol.* 14: 1125–1134.

46. Knubel, C. P., F. F. Martínez, R. E. Fretes, C. Díaz Lujan, M. G. Theumer, L. Cervi, and C. C. Motrán. 2010. Indoleamine 2,3-dioxigenase (IDO) is critical for host resistance against *Trypanosoma cruzi*. *FASEB J.* 24: 2689–2701.
47. Arocena, A. R., L. I. Onofrio, A. V. Pellegrini, A. E. Carrera Silva, A. Paroli, R. C. Cano, M. P. Aoki, and S. Gea. 2014. Myeloid-derived suppressor cells are key players in the resolution of inflammation during a model of acute infection. *Eur. J. Immunol.* 44: 184–194.
48. Sanoja, C., S. Carbajosa, M. Fresno, and N. Gironès. 2013. Analysis of the dynamics of infiltrating $CD4^+$ T cell subsets in the heart during experimental *Trypanosoma cruzi* infection. *PLoS One* 8: e65820.
49. da Costa, T. A., M. V. Silva, M. T. Mendes, T. M. Carvalho-Costa, L. R. Batista, E. Lages-Silva, V. Rodrigues, C. J. Oliveira, and L. E. Ramirez. 2014. Immunomodulation by *Trypanosoma cruzi*: toward understanding the association of dendritic cells with infecting TcI and TcII populations. *J. Immunol. Res.* 2014: 962047.
50. Giordanengo, L., S. Gea, G. Barbieri, and G. A. Rabinovich. 2001. Anti-galectin-1 autoantibodies in human *Trypanosoma cruzi* infection: differential expression of this beta-galactoside-binding protein in cardiac Chagas' disease. *Clin. Exp. Immunol.* 124: 266–273.
51. Roffê, E., A. G. Rothfuchs, H. C. Santiago, A. P. Marino, F. L. Ribeiro-Gomes, M. Eckhaus, L. R. Antonelli, and P. M. Murphy. 2012. IL-10 limits parasite burden and protects against fatal myocarditis in a mouse model of *Trypanosoma cruzi* infection. *J. Immunol.* 188: 649–660.
52. Randolph, G. J., J. Ochando, and S. Partida-Sánchez. 2008. Migration of dendritic cell subsets and their precursors. *Annu. Rev. Immunol.* 26: 293–316.
53. Hawiger, D., K. Inaba, Y. Dorsett, M. Guo, K. Mahnke, M. Rivera, J. V. Ravetch, R. M. Steinman, and M. C. Nussenzweig. 2001. Dendritic cells induce peripheral T cell unresponsiveness under steady state conditions in vivo. *J. Exp. Med.* 194: 769–779.
54. Belkaid, Y., and K. Tarbell. 2009. Regulatory T cells in the control of host-microorganism interactions. *Annu. Rev. Immunol.* 27: 551–589.
55. Montagnoli, C., A. Bacci, S. Bozza, R. Gaziano, P. Mosci, A. H. Sharpe, and L. Romani. 2002. B7/CD28-dependent $CD4^+CD25^+$ regulatory T cells are essential components of the memory-protective immunity to *Candida albicans*. *J. Immunol.* 169: 6298–6308.
56. Belkaid, Y., C. A. Piccirillo, S. Mendez, E. M. Shevach, and D. L. Sacks. 2002. $CD4^+CD25^+$ regulatory T cells control *Leishmania major* persistence and immunity. *Nature* 420: 502–507.
57. Amante, F. H., A. C. Stanley, L. M. Randall, Y. Zhou, A. Haque, K. McSweeney, A. P. Waters, C. J. Janse, M. F. Good, G. R. Hill, and C. R. Engwerda. 2007. A role for natural regulatory T cells in the pathogenesis of experimental cerebral malaria. *Am. J. Pathol.* 171: 548–559.
58. Kotner, J., and R. Tarleton. 2007. Endogenous $CD4^+$ $CD25^+$ regulatory T cells have a limited role in the control of *Trypanosoma cruzi* infection in mice. *Infect. Immun.* 75: 861–869.
59. Sales, P. A., Jr., D. Golgher, R. V. Oliveira, V. Vieira, R. M. Arantes, J. Lannes-Vieira, and R. T. Gazzinelli. 2008. The regulatory $CD4^+CD25^+$ T cells have a limited role on pathogenesis of infection with *Trypanosoma cruzi*. *Microbes Infect.* 10: 680–688.
60. Mariano, F. S., F. R. Gutierrez, W. R. Pavanelli, C. M. Milanezi, K. A. Cavassani, A. P. Moreira, B. R. Ferreira, F. Q. Cunha, C. R. Cardoso, and J. S. Silva. 2008. The involvement of $CD4^+CD25^+$ T cells in the acute phase of *Trypanosoma cruzi* infection. *Microbes Infect.* 10: 825–833.
61. Monteiro, A. C., V. Schmitz, E. Svensjo, R. T. Gazzinelli, I. C. Almeida, A. Todorov, L. B. de Arruda, A. C. Torrecilhas, J. B. Pesquero, A. Morrot, et al. 2006. Cooperative activation of TLR2 and bradykinin B_2 receptor is required for induction of type 1 immunity in a mouse model of subcutaneous infection by *Trypanosoma cruzi*. *J. Immunol.* 177: 6325–6335.
62. Monteiro, A. C., V. Schmitz, A. Morrot, L. B. de Arruda, F. Nagajyothi, A. Granato, J. B. Pesquero, W. Müller-Esterl, H. B. Tanowitz, and J. Scharfstein. 2007. Bradykinin B_2 receptors of dendritic cells, acting as sensors of kinins proteolytically released by *Trypanosoma cruzi*, are critical for the development of protective type-1 responses. *PLoS Pathog.* 3: e185.
63. Campetella, O., J. Martínez, and J. J. Cazzulo. 1990. A major cysteine proteinase is developmentally regulated in *Trypanosoma cruzi*. *FEMS Microbiol. Lett.* 55: 145–149.
64. Risso, M. G., G. B. Garbarino, E. Mocetti, O. Campetella, S. M. Gonzalez Cappa, C. A. Buscaglia, and M. S. Leguizamon. 2004. Differential expression of a virulence factor, the *trans*-sialidase, by the main *Trypanosoma cruzi* phylogenetic lineages. *J. Infect. Dis.* 189: 2250–2259.
65. Soares, R. P., A. C. Torrecilhas, R. R. Assis, M. N. Rocha, F. A. Moura e Castro, G. F. Freitas, S. M. Murta, S. L. Santos, A. F. Marques, I. C. Almeida, and A. J. Romanha. 2012. Intraspecies variation in *Trypanosoma cruzi* GPI-mucins: biological activities and differential expression of α-galactosyl residues. *Am. J. Trop. Med. Hyg.* 87: 87–96.